Magnetic Energy Losses and Pinning Forces in $Y_1Ba_2Cu_3O_7/Ag_2O$ High-T_c Superconductor

by

Esam Ibn Hamed Ahmad Abdul Hafidh

A Thesis Presented to the

FACULTY OF THE COLLEGE OF GRADUATE STUDIES

KING FAHD UNIVERSITY OF PETROLEUM & MINERALS

DHAHRAN, SAUDI ARABIA

In Partial Fulfillment of the
Requirements for the Degree of

MASTER OF SCIENCE

In

PHYSICS

June, 1996

MAGNETIC ENERGY LOSSES AND PINNING FORCES IN $Y_1Ba_2Cu_3O_7/Ag_2O$ HIGH- T_c SUPERCONDUCTOR

BY

ESAM IBN HAMED AHMAD ABDUL HAFIDH

A Thesis Presented to the

FACULTY OF THE COLLEGE OF GRADUATE STUDIES

KING FAHD UNIVERSITY OF PETROLEUM & MINERALS

DHAHRAN, SAUDI ARABIA

In Partial Fulfillment of the
Requirements for the Degree of

MASTER OF SCIENCE

In

PHYSICS

JUNE 1996

King Fahd University of Petroleum and Minerals

Dhahran, Saudi Arabia

College of Graduate Studies

This thesis written by Esam bin Abdul-Hafidh under the direction of his thesis advisor and approved by his thesis committee, has been presented to and accepted by the Dean, College of Graduate Studies, in Partial fulfillment of the requirements for the degree of Master of Science in Physics.

Thesis Committee:

Dr. Khalil A. Ziq (Chairman)

Dr. Abdulaziz S.Al-Harthi (Member)

Dr. M. M. Faiz (Member)

Dr. Nasser Hamdan (Member)

Approved by

Dr. Muhammad A.Garwan

Department Chairman

Dr. Al-Shehri, Abdulla

Dean, College of Graduate Studies

Date: June 18, 1996

ACKNOWLEDGMENT

Thanks to Allah the cherisher and the sustainer who made it possible for me to finish this research with patience.

Thanks to King Fahd University of Petroleum and Minerals which gave me every opportunity for this achievement since my admission for B.Sc. and then through the Master program.

Thanks to all the many people who have given me help, encouragement, support and advice during this project. Among them, I would like to express my warmest thanks to Dr. Khalil A. Ziq, my thesis adviser who gave me invaluable help and full guidance in ways of tackling the difficulties encouragement during various stages of this project. I shall always remember these early morning experiments during the summer of 1995. I must also thank Dr. Mohammad Garwan - the chairman of physics department, all faculty, and members of the department.

Thanks also to the thesis committee which consists of Dr. M. Faiz, Dr. Nasser Hamdan, Dr. Abdulaziz S. Al-Harthi. Thanks and appreciation to Dr. A. Saif for his various helps during the writing of this thesis.

Finally, I must give my thanks to Mr. Abdullah Al Bashrawi and his

colleagues in the Cryogenic Lab. for helping me with LHe and LN_2 which are important for the completion of the experimental aspects of this research project.

Contents

List of Tables

List of Figures

خلاصة الرسالة

الاسم الكامل : عصام بن حامد بن أحمد بن عبد الحفيظ

عنوان الدراسة : فقد الطاقة المغناطيسية والقوى المثبتة في $Y_1Ba_2Cu_3O_7$ مفرط التوصيل ذي درجة حرارة حرجة عالية.

التخصص : فيزياء

تاريخ الشهادة : يونيو ١٩٩٦م

تعنى هذه الدراسة باستخدام القياسات المغناطيسية لتوصيف تغير التيارات الحرجة والقوى المثبتة وفقد الطاقة تبعا لتغير عدة عوامل مؤثرة على عينات من المادة مفرطة التوصيل $Y_1Ba_2Cu_3O_7$ ذات مواصفات عاليـــة.

سجلت هذه القياسات عند تغير عدة عوامل هي :

(١) مقدار المجال المغناطيسي

(٢) درجة الحرارة

(٣) إضافة كميات مختلفة من أكسيد الفضة Ag_2O

ظهر من خلال الدراسة أن إضافة أكسيد الفضة بنسب وزنية أقل من ١٠% إلى $Y_1Ba_2Cu_3O$ يؤدي إلـــى ازدياد في قيم القوى المثبتة وقيم التيارات الحرجة والقوى المثبتة بالتناقص عند زيادة نسبة أكسيد الفضة لأكثر من ١٠% حيث يستمر ذلك إلى أن تصبح النسبة ٥ % فيظهر أن العينة وإن كانت لا تزال فائقـــة التوصيـــل لكنها ذات مواصفات ضعيفة من ناحية قيمة التيار الحرج الذي يمكن أن تتحمله.

أما بالنسبة لفقد الطاقة فقد كانت دراستها في حالة تسليط مجال مغناطيسي مســـتمرDC خلافـــا لكثـــير مـــن الدراسات التي ركزت على المجال المغناطيسي المتناوب AC من حيـــث اعتمادهـــا علـــى قيمـــة المجـــال المغناطيسي المستعمل وعلى درجة الحرارة مما يبين أهمية دراستنا هذه.

بداية تزداد كمية الطاقة المفقودة زيادة ملحوظة بازدياد قيمة المجال المغناطيسي. وعندما تزداد قيمة المجـــال عند قيمة محددة(H_p) يتناقص معدل الزيادة في الطاقة المفقودة، وفي جميع العينات ظهر سلوكا عاما مشابـــها لسلوك العينة التي تحتوي على نسبة من أكسيد الفضة تساوي ١٠% مظهرة سلوكا يقترب من التشبع.

كما تم دراسة سلوك كميات الطاقة المفقودة تبعا لتغير درجة الحرارة وتأثير ذلك على كل من الطاقـــة الكليـــة ومكوناتها المحتبس والديامغناطيسي. تبين من خلال ذلك أن الشق الديامغناطيسي يمثل الشق الأكبر للفقد بينما المحتبس يسبب الفقد بنسبة قليلة وعند درجات حرارة عالية فوق ٣٠ كلفن في الغالب. عند درجـــات حـــرارة منخفضة دون ٣٠كلفن فإن خطوط التدفق المحبوسة تؤثر بشكل واضح مع القسم الديامغناطيســـي فـــي فقـــد الطاقة.

درجة الماجستير في العلوم
جامعة الملك فهد للبترول والمعادن
الظهران، المملكة العربية السعودية
يونيو ١٩٩٦م

ABSTRACT

NAME : ESAM IBN HAMED AHMAD ABDUL HAFIDH

TITLE : MAGNETIC ENERGY LOSSES AND PINNING FORCES IN $Y_1Ba_2Cu_3O_7$ Hi-T_c SUPERCONDUCTOR

MAJOR : PHYSICS

DATE : JUNE 1996.

Magnetic measurements have been conducted on $Y_1Ba_2Cu_3O_7/(Ag_2O)_x$ for x ranging between 0% and 50% weight ratio. The major quantities which were under the scope of this project are: the critical current density J_c, pinning force F_p and the energy loss W. The temperature and field dependance of the critical current densities, pinning forces and energy losses of $Y_1Ba_2Cu_3O_7/(Ag_2O)_x$ system were investigated in this study.

The addition of $(Ag_2O)_x$ with $x \leq 10\%$ was found to increase J_c and F_p, while for $x > 10\%$ a reduction in both values have been found at all temperature studied. At x=50%, however the sample even though is still superconducting , but have a deteriorated magnetic properties, with a very low critical current density. For all samples in this study, the energy loss has been found to strongly depend on the magnetic field at low fields, while it reaches saturation for fields

above the full penetration field.

The contribution to the energy loss due to the trapped flux and due to the diamagnetism, decreases strongly with temperature. The loss is mostly diamagnetic at high temperatures >30K, while at <30K both (diamagnetic and trapped) flux lines contribute to the dissipation of energy.

MASTER OF SCIENCE DEGREE

KING FAHD UNIVERSITY OF PETROLEUM AND MINERALS

Dhahran, Saudi Arabia

JUNE 1996

Chapter 1

Introduction

1.1 Discovery

The pioneering work of H. Kamerlingh Onnes of liquefying helium in 1908 made it possible to conduct physical experiment at temperature down to 4.2 K. One of the first experiments that Onnes performed at low temperature was to measure the resistance of elemental mercury with decreasing temperature. He noticed a sharp drop in the resistance at about 4K, the resistance dropped almost to zero. He called this phenomena "superconductivity". After discovering superconductivity in Hg (at 4.15K), it had been found that many elements and a number of alloys become resistanceless "**superconductor**"when cooled through their transition temperatures T_0 [1]. Zero resistance is the first char-

acterizing property of superconducting materials.

In addition to that, superconductors are perfectly diamagnetic materials. Cooling the sample in the presence of small magnetic fields, lower than H_c, superconductors do not allow any magnetic fields to penetrate them and the field is completely expelled out. This is known as the Meissner effect [2].

Performing experiments at liquid nitrogen temperatures rather than liquid helium is an attractive idea due to the economical and preperation procedure ease of LN2 rather than LHe. This has motivated scientists to look for superconductors with higher transition temperatures. Before 1986, the highest transition temperature ever achieved for conventional superconductors is that for Nb_3Ge with T_c=22.3°K [2].

Recently, Bednorz and Muller in 1986 have discovered a new type of materials that exhibit superconductivity at about 35K [3]. The new ceramic material is lanthanum barium copper oxide (LaBaCuO) and has perovskite structure. Substitution of Sr instead of Ba raises T_c to about 40K [4].

Superconducting materials of transition temperature above liquid nitrogen (77K) was first discovered by M. K. Wu et al. at the University of Alabama and C. W. Chu at the University of Houston, Wu et al. have found that substituting Y in place of La has increased T_c dramatically above liquid nitrogen temperature, to reach above 90K[3]. The new ceramic superconductors has

the chemical formula $Y_1Ba_2Cu_3O_{7-\delta}$ with $T_c \approx 92K$. This discovery was soon followed by another two new ceramic families with even higher transition temperature : Bi-Sr-Ca-Cu-O and Tl-Ba-Ca-Cu-O compounds with $T_c \approx 110K$ and $T_c \approx 118K$, respectively [4]. Recently, a new family has been added to the list of ceramic high-Tc superconductors; it is Hg-based SC with a transition temperature ranging from 90 - 135 K. These materials are known as high temperature superconductors and abbreviated as HTSC [4].

1.2 Basic Properties of HTSC

The most important characterizing properties of superconductors can be summarized as: 1. The electrical resistance of a superconductor below the transition temperature is zero, and 2. A superconductor is a perfect diamagnet.

The transition temperature can be determined using either of these two characterizing properties, namely, (i) measuring the resistance versus temperature in the absence of any applied field. The resistance generally decreases gradually with temperature until the temperature is very close to their transition temperatures where it drops sharply. These materials goes to a superconducting state and lose their electrical resistance at the transition temperature. (ii) Measuring the magnetization in the presence of small magnetic field as a

function of temperature also reveals the superconducting nature at the transition temperature T_c. According to Meissner effect , we have :

$$B = H + 4\pi M = 0$$

or

$$M = -\frac{1}{4\pi}H$$

which means that, in the superconducting state, the magnetization is opposite and proportional to the applied magnetic field and has a slope equals to $-\frac{1}{4\pi}$. The temperature at which the magnetization becomes zero is the transition temperature after which the magnetization becomes positive and the material goes to normal state .

Conventional and HTSC share many common superconducting properties. For example, flux quantization, Josephson tunneling, presence of energy gap, and the jump in heat capacity at $T=T_c$ [2]. However, HTSC (or cuprates) have some unusual properties such as their transition temperature is commonly higher than liquid nitrogen boiling point, facilitating many applications and basic research to be performed without economical difficulties associated with liquid helium. HTSC also sensitive to the amount of oxygen present in the sample. For example, $Y_1Ba_2Cu_3Ox$ has a transition temperature above 90 K for $x \sim 7$; it reaches 55K if the number of oxygen atoms per unit formula is

reduced to ~6.5 [4].

There are two characteristic geometrical length, that helps understanding many of the superconducting properties. First, the London penetration depth λ, the depth to which the flux of the applied magnetic field penetrates the superconducting material at temperature below T_c [1]. The surface currents in a superconductor flow within the penetration depth which vary for different materials. The current density in a superconductor is related to the vector potential through the following relation :

$$\overrightarrow{J} = -\frac{1}{4\pi\lambda^2}\overrightarrow{A}$$

from which, we can obtain [5] :

$$B = B_0 e^{-\frac{x}{\lambda}}$$

and

$$J = J_0 e^{-\frac{x}{\lambda}}$$

where B_0 and J_0 are the flux density and the critical current density at the surface of the superconductor respectively.

Second, the coherence length ξ introduced by Pippard which is defined as the probability of finding an electron with momentum $-\overrightarrow{P}$ and spin down in a volume element $d\tau_2$ at a distance r from a volume element $d\tau_1$ which

contain an electron with momentum $\overrightarrow{P}$ and spin up. For conventional type-I superconductors, ξ is of the order of 10^6, while for HTSC it is very small and in the range of $0.5 - 30$ [1] .

For any superconductor, it is found that the ratio of the penetration depth to the coherence length (Ginzburg-Landau constant) expressed as $\kappa = \frac{\lambda}{\xi}$ is a characteristic value that can be used to classify superconductors as known as type-I or type-II in the following manner :

1. if $\kappa < \frac{1}{\sqrt{2}}$the superconductor is type-I and
2. if $\kappa > \frac{1}{\sqrt{2}}$, it is type-II.

In HTSC, the coherence length ξ is much shorter than the penetration depth λ such that all HTSC cuprates are type-II superconductors with very high values of Ginzburg-Landau constant. The flux lines are weakly pinned compared to conventional superconductors. However, to be used in practical applications, imperfections and pinning centers have to be added to these new ceramic HTSC, so that they can carry higher critical currents [4]. Usually superconductors are charecterized by a lower critical field H_c1 and an upper critical field H_c2.

HTSC also have very high value of the upper critical field. A typical value of H_{c2} range between 80 and 200Tesla at very low temperature ($\sim$ 4K). This is about an order of magnitude higher than that for conventional superconduc-

tors. However, the critical currents in HTSC are lower than the corresponding values found in conventional SC [3], even at a very low temperature (~4K).

1.3 Crystal Structure

A knowledge of the structure is crucial to understand many superconducting properties of these high temperature superconductors [6]. The crystal structure pattern of HTSC systems has large anisotropy and differ from other known superconducting structures [7]. This structural anisotropy is reflected in many superconducting properties of HTSC. The structure of $Y_1Ba_2Cu_3O_{7-\delta}$ is orthorhombic and is shown in Fig (1.1) which shows the following features, common to most HTSC.

1. There are Cu-O planes and Cu-O chains.

2. The structure is based on the simple cubic perovskite consisting of three such cells stacked one upon the other. The number of Cu-atoms per formula unit determines the number of cells or Cu-layer in the structure.

3. The yttrium and barium are on the *corners* and alternate in Ba-Y-Ba-Ba-Y-Ba sequence

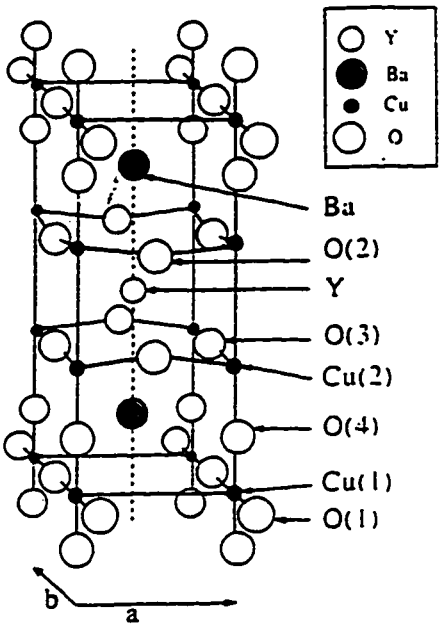

Figure 1.1: The orthorhombic crystal structure of $Y_1Ba_2Cu_3O_{7-\delta}$

4. Oxygen vacancies : no oxygen in the yttrium plane and two oxygens missing from the Cu-O layer between barium planes.

1.4 Magnetic Properties

Superconductors are diamagnetic materials. In 1933, Meissner and Ohsenfeld measured the flux distribution inside tin and lead samples which were cooled to below $T_c$in a magnetic field less than the critical field H_c. It was found that all flux inside were cancelled and the samples became perfectly diamagnetic. They

summarize their result as : "a metal in the superconducting state never allows a magnetic flux density to exist in its interior" [1]. This effect was later known as Meissner effect. If the applied field exceeds H_{c1}, the material goes to normal state. This type of superconductors is known as type-I superconductors(with $\kappa < \frac{1}{\sqrt{2}}$).

Type-II superconductors are characterized by the presence of an upper critical field H_{c2}, above which the superconducting material becomes normal conductors. For field values between $H_{c1}$and H_{c2}in type-II, the superconductor is in a mixed state of normal and superconducting regions or trapped flux state. If a superconductor is cooled below its transition temperature in the presence of a magnetic field, the field lines will be expelled outside, and flux lines are trapped by defects. However, non-ideal superconductors contain large number of defects, that will trap the flux line when cooled below $T_c$in the presence of any value of the magnetic field. The resulting state is called field cooled state(FC). On the other hand, if a superconductor is cooled below $T_c$in zero magnetic field and then a magnetic fields is applied (Zero FC or ZFC state), the net internal flux remains zero [1]. It turns out that these two states are totally different, since in the FC, there is some flux trapping in the sample and at low temperatures, the total magnetization (diamagnetic and trapped) may add to give positive value. However, when the trapped magnetization is

subtracted from the total value, it is concluded that the superconducting phase survives at low temperature [9]. If a superconductor contains many pinning centers, the situation is different and the flux trapping occurs for both (ZFC) and (FC) states [9].

1.5 Critical Current

The minimum current density that can be passed along a piece of a superconductor and transform it to normal state is called the critical current density [1] resistance, since on passing a current through the sample, the motion of the flux lines induces a potential difference across it. It is of great technological interest to understand the mechanism which controls the critical current .

For practical purposes , it is desired to be able to produce currents as large as possible without destroying the superconducting state. The microstructure and the metallurgical state affects both the magnitude and the anisotropy of the critical current. For example, reducing the grain size, creating new defects by doping or through irradiations with fast neutrons, protons, ... etc. are known to enhance the values of the critical current densities J_c[8].

Experimentally, $J_c$can be measured using transport measurements, a one microvolt ($1\mu V$) is often used to define the corresponding current as a critical

current. Critical current density can be evaluated using magnetic measurements, the hysteresis loops and Bean's model. In this work we will be measuring the hysteresis loops for Y_{123}/Ag_2O and using Bean's model to evaluate the critical current density upon varying temperature, field, and silver oxide concentration. The behavior of the critical current with field and temperature will be discussed in chapter 3.

1.6 Pinning force

The critical current density is a totally dependent quantity on the pinning mechanism of a superconductor.

Point defects, impurities, inhomogeneity, and dislocations are commonly found in most conventional and all high transition temperature superconductors. These imperfections create what is commonly known as pinning centers. In the presence of applied magnetic field, these pinning centers prevent vortex lines from moving under the influence of varying magnetic field or transport current and cause irreversibility in the magnetization when monitored as the applied magnetic field changes. This give rise to various hysteresis effects; and hence to energy losses [10].

For a superconductor in a mixed state, the vortices are pinned at imper-

fections of the material with these normal core pinned at the imperfection site by certain pinning force that hold the vortices in place [1]. These normal cores start moving when the Lorentz force exceed the pinning force [11]. The width of the hysteresis loop is related to the strength of pinning forces.. According to Bean's model, the width of the hysteresis loop is proportional to the critical current density, then the critical current density is proportional to the defect density. For practical purposes, it is always desired to get higher and higher critical currents at elevated temperatures such as liquid nitrogen boiling point[12].

Scaling of the pinning forces, enables us to better understand the behavior of the pinning forces with field, temperature and defect density. Moreover, based on scaling arguments, we can predict the behavior of these pinning forces under extreme conditions. For all temperatures lower than the superconducting transition temperature, Lorentz forces and also the pinning force $F_p$increases as H and $J_c$increase until it reaches a maximum F_{max}at field H^*, then start decreasing approaching zero asymptotically. This is due to the fact that as H increases, $J_c$decreases. All the curves of pinning force versus field at different temperatures fall on a single curve if scaling rules such as that introduced by Fiets and Webb in 1969 is applied[10].

These curves are found to obey a general scaling form

$$Fp = \alpha(D) \cdot H_{c2}^{n} \cdot f(b)$$

where $b = H/H_{max}$, $\alpha(D)$, $n$are material dependant and $f(b)$is a function only of the reduced field b. Scaling of the pinning forces for all our samples will be discussed in chapter 3.

1.7 Energy Loss

Large-scale applications of HTSC are strongly limited by the magnitude of the electrical current density that can be transported through the material with no energy losses [13]. The area enclosed by the hysteresis loop for a certain temperature is the energy loss (hysteretic loss) during a cycle [14]. Other sources of dissipation such as those related to eddy currents (viscous losses) and to flux penetration across the surface do not seem to play an important role [15, 16]. In this project, we are going to study the total hysteretic loss by evaluating the area of the hysteresis loops at different fields and temperatures. Energy losses in Y/Ag2O composite will be stated in chapter 4 along with related properties

1.8 Y_{123}/Ag_2O composites

Material applications such as magnets, transmission lines for electricity .. etc. require improved ductility and fracture toughness in HTSC ceramic materials. Characterization and easy control of these materials require the addition of metals to these ceramic superconductors. Among the various metals, it has been found that the addition (not substitution) of silver to the already reached HTSC improves both mechanical and superconducting properties. First, it fills the intergranular space (holes). Second, the transition temperature is not affected much for silver concentration $\leq$ 10% wt ratio. Third, the normal state resistivity of Y_{123}/ Ag_2O decreases with increasing silver concentration. In addition to that, the critical current of the composite is enhanced due to additional pinning centers produced by silver imperfections at the grain boundaries. Silver addition is of great technological interest [17, 18, 19].

1.9 Statement of the problem

For practical applications of HTSC, a further improvement of their magnetic and electrical properties is needed. The critical current density J_c of Y123 is high enough at liquid Helium temperature in the presence of high external applied magnetic field H, but it is still low at liquid nitrogen temperature. To

overcome this problem, it is necessary to introduce effective pinning centers and deepen the pinning mechanism in HTSC [1, 3].

One way of enhancing the pinning forces, and consequently the critical current density is by forming composites of Y123 and Ag or Ag_2O. In this project, we are going to study the behavior of these pinning forces in Y123 sample for different addition of silver oxide(Y123/Ag_2O).

In addition, not very much information is available about the magnetic energy losses and remanent magnetization in these Y123/Ag_2O composites among many other properties. We also propose to investigate the effects of Ag_2O on the energy losses and remanent magnetization in these high-T_c composite ceramics.

Chapter 2

Experimental Technique

Measurements were performed using a fully computerized Lakeshore-PAR Vibrating Sample Magnetometer (VSM) system (Model 4500/150A)

The VSM measures the total magnetic moment of a particular material under investigation. The sample is made to undergo sinusoidal vertical vibration in the direction of the applied magnetic field. An electrical signal is induced in two suitably located stationary pick-up coils which are wound in opposite direction to give a maximum reading .

The major components of the system are :

1. The cryostat

2. The cryomagnet electronic console which include :

- (a) Power supply model Lakeshore 612

  which can be programmed to either constant current (cc) or constant voltage (cv) operation with the capacity to source or sink up to 1000 VA. Maximum outputs are $\pm$ 125 A and $\pm$ 3V. Unlike conventional designs, voltage and current flow are bidirectional. Sink power is returned to the AC line as opposed to being wasted by an energy absorber in the form of excessive heat in conventional power supplies.

  (b) Power supply controller model Lakeshore 601, it includes:

  (a) 1. computer interface module

  2. LHe level meter

  3. Gaussmeter

  (c) Temperature controller model Lakeshore DRC-91CA

  which contain two sensors inside the cryostat (carbon - glass and platinum) for automatic temperature control over temperature range 2-300K.

  (d) VSM controller model 4500

  which contain different sections at its front panel from which the system is controlled. For example, EMU range section, Oersteds,

Sweep generator , Temperature control, etc.

(e) Superconducting coil: it generates longitudinal magnetic field up to 9 Tesla.

2.1 Sample Preparation

Solid state reaction method is used to prepare good quality single phase samples of Y123 that show sharp transition to zero resistance and strong magnetic levitation. Starting with Y_2O_3, $BaCO_3$, and CuO of purities 99.999 %, the powder was well mixed for about an hour (dry and wet mixing). The mixture was then placed in a furnace for calcination at 900°C for about 24 hours. After cooling, the mixture was reground and then formed into small pellets (13mm in diameter and about 2-3mm thick) under the pressure of 3000 kg/cm^2. Finally, the pellets were annealed in flowing oxygen at temperature of 950°C. The temperature was then reduced to 550-600K and the samples were kept for another 24 hours then furnace-cooled to room temperature [6, 17].

For Y123/Ag_2O composite samples, an appropriate weight ratios of Y123 powder and silver oxide (Ag_2O) were mixed and annealed at 900°C for 10-24 hours in oxygen, then cooled to about 550°C where they have kept for about 24 hours in flowing oxygen. Finally the sample were furnace cooled to room

Table 2.1: The variation of the transition temperature with silver oxide content

sample	wt. of Ag_2O (%)	T_c (K)
Y123	0	91.7
YAg14	7.14	91.5
YAg10	9.52	90.8
YAg7	14.29	90.4
YAg25	25	80.7
YAg50	50	80

temperature.

All superconducting samples have been characterized by measuring magnetization M vs temperature T. The weight ratios of Y123 to Ag_2O and the percentage of silver oxide for the samples used in this study are shown in Table 2.1 along with their corresponding superconducting transition temperatures T_c.

The variation of the transition temperature with silver oxide content is shown in Fig(2.1).

2.2 Experimental Procedure

As described in chapter 1, two kinds of magnetic measurements can be performed, namely, field cooled (FC) where the sample is cooled below the transition temperature T_c in the presence of any value of the magnetic field, and zero field cooled (ZFC) where the sample is cooled to below the transition temperature in zero applied field. All of our measurements where performed in (ZFC) state, were full hysteresis loops were obtained by measuring the magnetization (M) in different fields and temperatures by cycling the field up to ± 9.

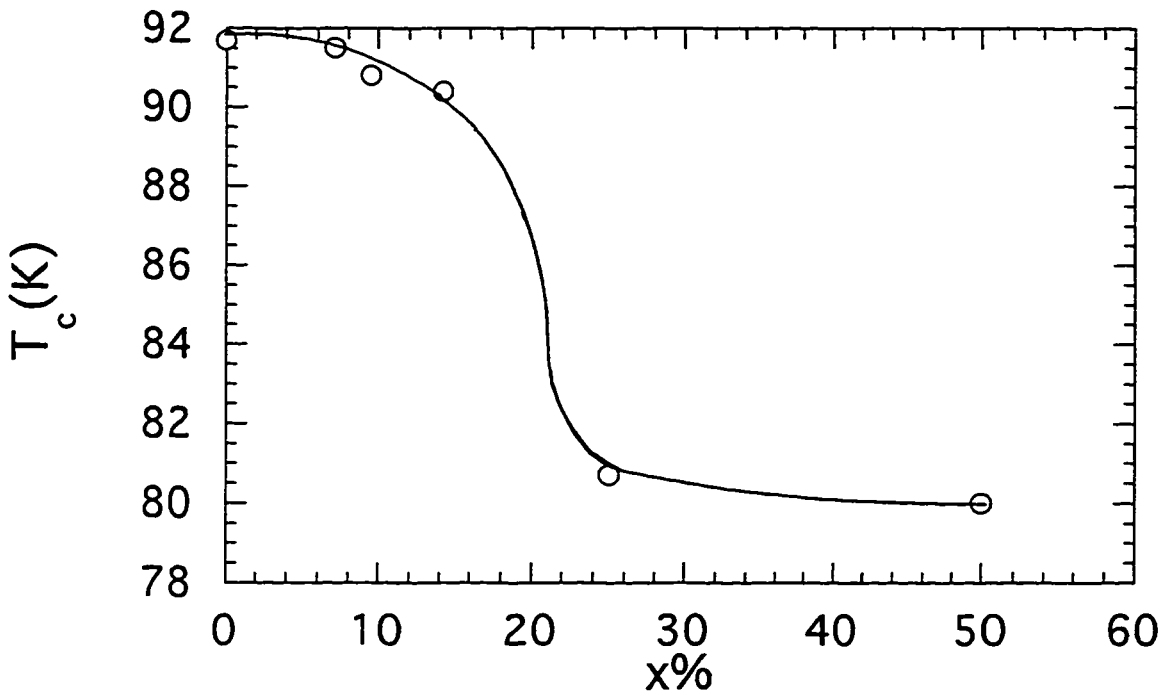

Figure 2.1: Silver oxide effect on the transition temperature

Chapter 3

Critical Currents and Pinning Forces

3.1 Introduction

Magnetic characterization of superconductors is commonly done by either measuring the flux density B in the sample, or measuring the magnetization of the sample M upon changing temperature, field and history. In this research, the magnetization measurements technique is used in which the induced voltage V_i in pickup coils of N-turns surrounding the sample is measured. The flux change ($\Delta\Phi$) in a specimen of cross-section A_s equals to the time integral of

the induced voltage. Using faraday's law we have :

$$N\Delta\Phi = -NA_s\Delta B = \int_{t(H=0)}^{t(H=H_0)} V_i(t')dt' \tag{3.1.1}$$

but

$$M = B - \mu_0 H_0 = -\frac{1}{NA_s}\int V_i(t')dt' - \mu_0 H_0 \tag{3.1.2}$$

where M is the magnetization (averaged over the specimen cross-section A_s

A lot of information about the magnetic characteristic of the sample can be deduced from the relation 3.1.1, and consequently from the hysteresis loops of the sample. Evaluation of the integral in equation 3.1.1 is done electronically and the magnetization is represented as voltage signal which is calibrated against a standard Ni-sample of known magnetization. However, the situation is greatly simplified if the hysteresis of the magnetization is small [10].

Hysteresis loops result from defects which involve imperfections of another substance voids, or chains of displaced atoms[1]. The HTSC in a mixed state is a superconducting bulk with a lattice of normal cores (or vortices). The motion of the vortices in the bulk is very much affected by presence of defects and any amount of foreign material introduced to Y_{123}[20, 21, 22].

3.2 Effect of the Magnetic Field and Temperature on The Shape of The Hysteresis Loops

The drastic change of the shape of the hysteresis loop is due to the motion of the vortices. Initially and for small cycling magnetic field lower than H_{c1} hysteresis is minimal and the magnetization is almost reversible. The hysteresis loop gets wider as the applied fields is increased until the field get to an intermediate penetrating value H_p. M Oussena et al. have shown that the width of the hysteresis loop decreases when the applied field overcomes H_p [21, 22]

For Y_{123} and above H_p and at low temperature ($< 10K$), the hysteresis loop width is almost independent of field, it becomes strongly field dependent at higher temperatures [23]. Similarly, Kim et al. have shown that J_c behaves differently below and above a characteristic temperature of 25°K for $Bi_2Sr_2CaCu_2O_x$(it will come in section 3.3 the relation between Jc and M which is extracted from hysteresis loops). Near the lower critical field (H_{c1}), Nelson [24] and Houghton [25] have suggested the possibility of entanglement and melting in the vortex state. Even when the vortices melt, a non-zero critical current has been observed by both magnetic[26] and transport[27] measurements.

This is an indication that at the melting point, the vortices are still pinned

(weakly) and the bulk is a superconductor [28]. However, near the upper critical field H_{c2}, and near T_c; another possibility of vortex melting transition is the glass phase transition, which was suggested by Fisher et al. [22, 29, 30].

3.2.1 General Behavior of The Hysteresis Loops

The three hysteresis loops shown in Fig.3.1 for pure Y_{123} sample at three different temperatures represent three regimes in which the shape of M(H) is distinctly different. At high fields($\geq$ 2 Tesla) and low temperatures ($4K$), the width of the loop ΔM is almost field independent up to the maximum field (9 Tesla) accessible in our system.

A maximum seen in ΔM below 1 Tesla and at low temperatures ($4.2K$) is observed commonly described as fishtail shaped of the hysteresis loop. Its magnitude and location decreases in field, with increasing temperature. As the temperature increases, ΔM is reduced further, but above the central peak ΔM, is nearly field independent. Still at higher temperatures $\geq 60K$, ΔM becomes strongly field dependant until the hysteresis loop collapses above certain irreversible field H_{irr}(Fig. 3.1). The fishtail shape of the loop has been studied by many others, for example, A Fert et al.[21] have attributed its shape to oxygen deficient regions in the sample. They found that the fishtail tend to disappear as the oxygen content is improved.

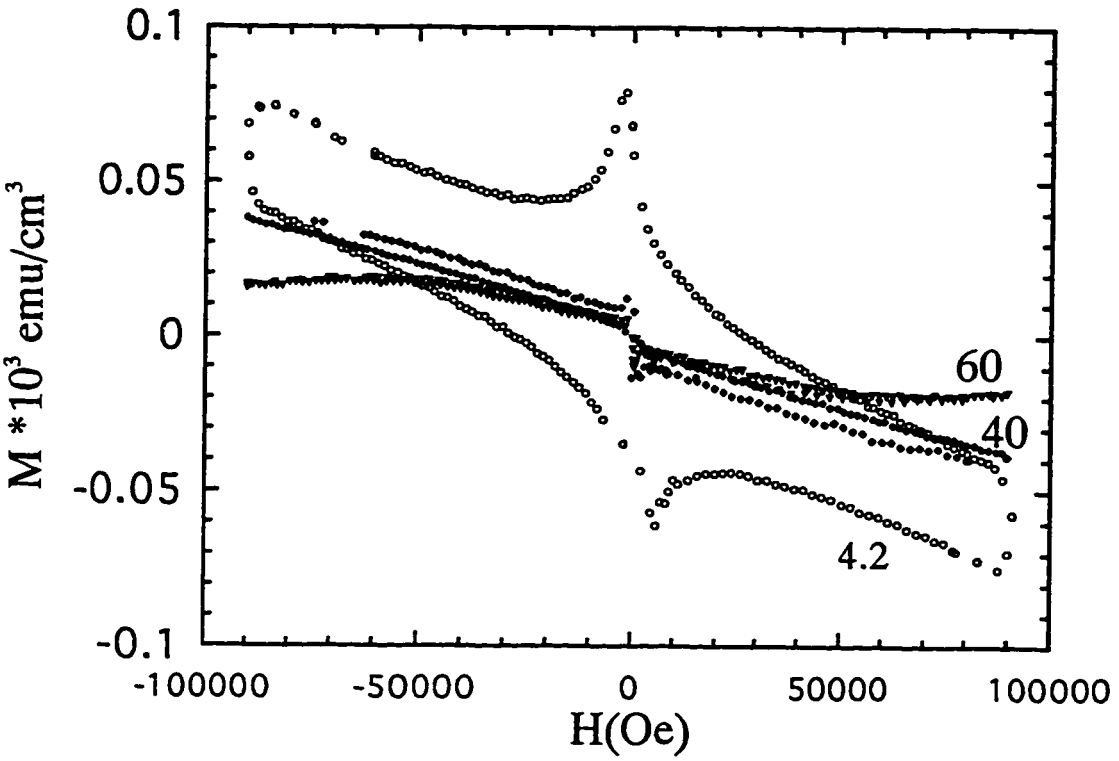

Figure 3.1: Hysteresis loops, M vs H for Y123, T=4.2K,40,60 respectively

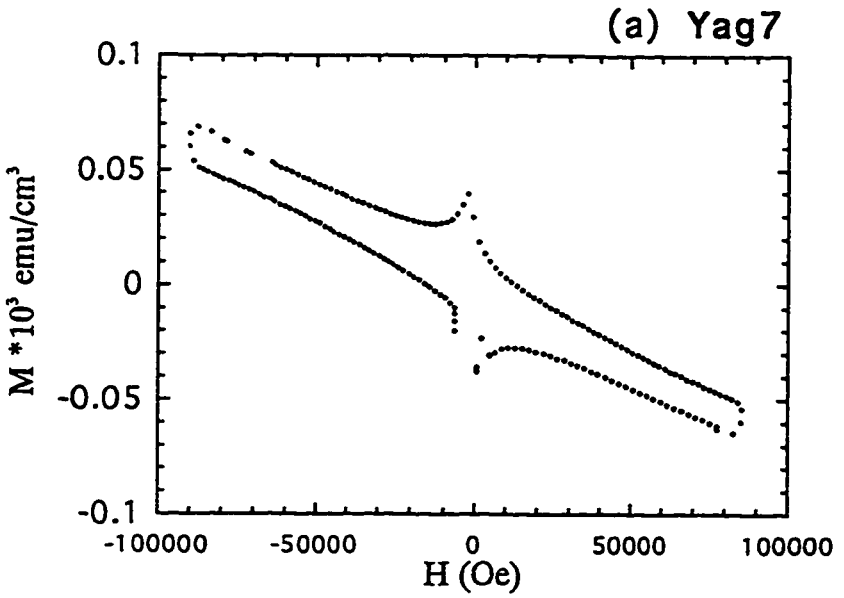
(a) Yag7
0.1
0.05
0
-0.05
-0.1
M *10³ emu/cm³
-100000
-50000
0
50000
100000
H (Oe)

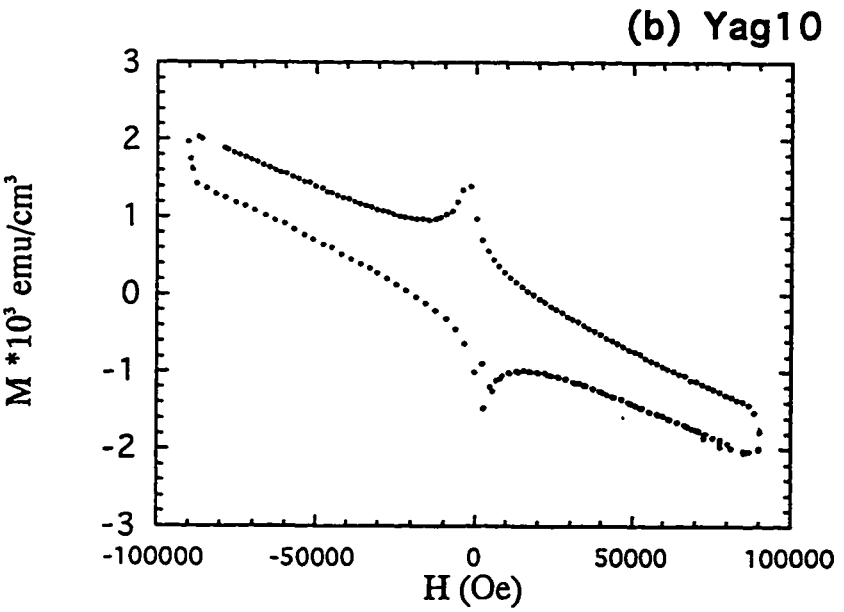
(b) Yag10
3
2
1
0
-1
-2
-3
M *10³ emu/cm³
-100000
-50000
0
50000
100000
H (Oe)

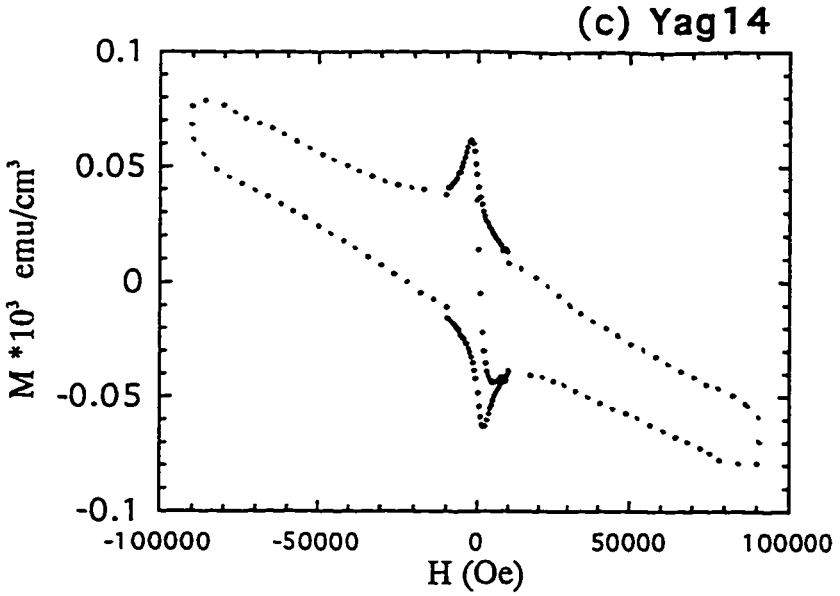
(c) Yag14
0.1
0.05
0
-0.05
-0.1
M *10³ emu/cm³
-100000
-50000
0
50000
100000
H (Oe)

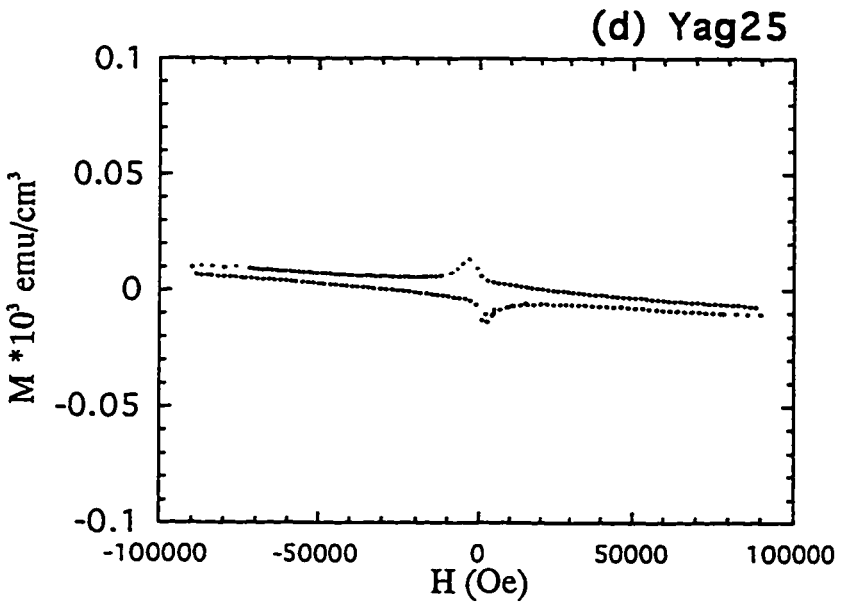
(d) Yag25
0.1
0.05
0
-0.05
-0.1
M *10³ emu/cm³
-100000
-50000
0
50000
100000
H (Oe)

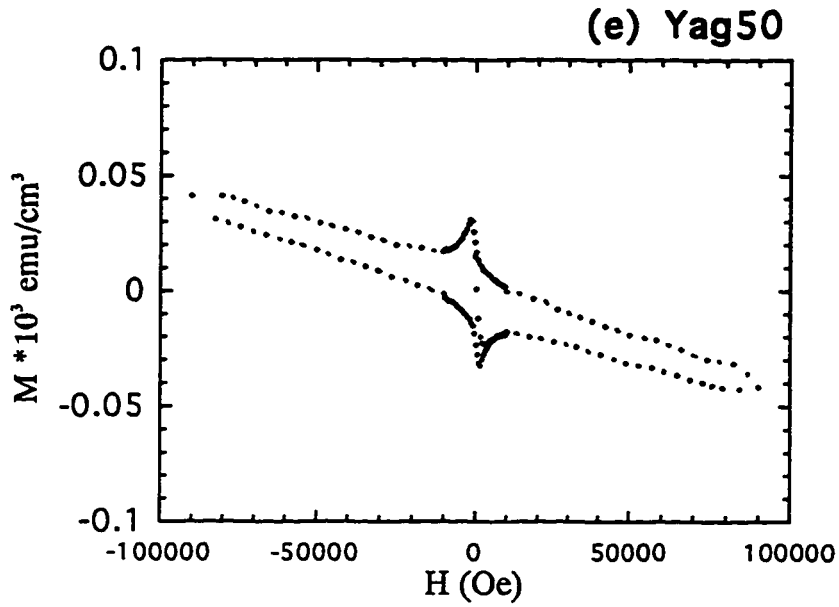

Figure 3.2: a,b,c,d,e: Hysteresis loops, M vs H for Y123 /(Ag2O)x, for x=7,10,14,25,50 at T=4.2K.

The shape of the hysteresis loop provide valuable information about the magnetic properties of the sample. Foreign materials when added to Y_{123} affect very much the shape of the hysteresis loops. Also , it has been shown that the width of the hysteresis loops increases as the density of the imperfections is increased until it reaches a maximum value above which J_c start decreasing [31]. This similar to what we have seen in Y_{123}/Ag_2O as shown in Fig. 3.3, where we present different hysteresis loops at 4.2K and cycling field between $\pm$9Tesla.

At 4.2K , for different content of Ag_2O added to Y_{123} less than 50%. All the hysteresis loops behave similar to loops observed for the pure Y_{123} . The width of the hysteresis loops first increases as the amount of Ag_2O increases up to about 10%(weight ratio). When silver content exceed 10%, the width start decreasing. This can be seen clearly in the behavior of the critical current $J_c(\propto \Delta M)$, where it reaches a maximum at about 10% wt percent of Ag_2O, and will be discussed in the following sections.

Finally, we should mention here that the shape of the sample may affect the shape of the hysteresis loop [32]. Furthermore, M. Oussena et al. have been studying the possibility of scaling of the hysteresis loops. They have shown that hysteresis loops showing the peak effect (or fishtail effect) are found to scale

with the width of the crystal [33].The relation of the shape of the hysteresis loops and the energy loss will be discussed in chapter 4.

3.3 Bean's Model "The Critical State Model"

The measured width ΔM of the hysteresis loops is related to the critical current J(H,T) through Bean's "critical" state model. In fact, it can be used to explain many of the properties of type-II superconductors. The model was independently introduced by Bean (1962) and London (1963), and is commonly referred to as Bean Model. It describes the variations of magnetization within a superconducting sample. Although, Bean based his model on some basic assumptions. It is now viewed as a consequence of the mixed state of type II superconductors [34].

The assumptions incorporated in the model are [34, 35]:

i) A filamentary mesh structure of the superconducting sample

ii) The applied field is small compared to the upper critical field H_{c2} and J_c is independent of field.

iii) The critical current density is independent of time (or in other words : the thermally activated flux creep should be greater than a lower critical value of about $40k_B$ T) [36].

iv) The sample exhibit large amplitude displacements of the flux vortices (at least one-quarter of a vortex spacing) [34, 35, 37], so that the motion of the vortices is irreversible, which in turn generates certain width of the hysteresis loop.

In general , to calculate the critical current density from hysteresis loops, two main models are commonly used. The first was developed - as described above - by Bean and is characterized by a hysteresis loop which has weak - field dependence, and J_c is field independent and is given as :

$$J_c = \frac{30\Delta M}{A} \tag{3.3.3}$$

where $\Delta M = M^+ - M^-, M^+(H)$ and $M^-(H)$are the algebraic values of the magnetization on the descending and ascending branches of the hysteresis loop at certain value of H and A is samole cross section.

However, if the critical current density is field dependant, the second model developed by Kim, Hempstead and Strand (KHS) commonly known as the critical state model is used to evaluate J_c through the relation :

$$J_c = \frac{\alpha}{\left|\widetilde{B}(r)\right| + B_0} \tag{3.3.4}$$

where $\widetilde{B}(r)$ is the flux density in the material, and α and B_0 are parameters

usually evaluated by fitting eqn. 3.3.4 to the hysteresis loops shown in Fig. 3.1 &3.2 [38]. These figures show typical hysteresis loop in our measurements and reveals that J_c is strongly field dependent at high temperatures and high field. At low fields, J_c is also field dependent at all temperatures, However, at high fields and low temperatures J_c is field independent, and therefore, it is not possible to get a satisfying fit using (KHS) over the whole range of T and H, and consequently Bean model is valid in this case.

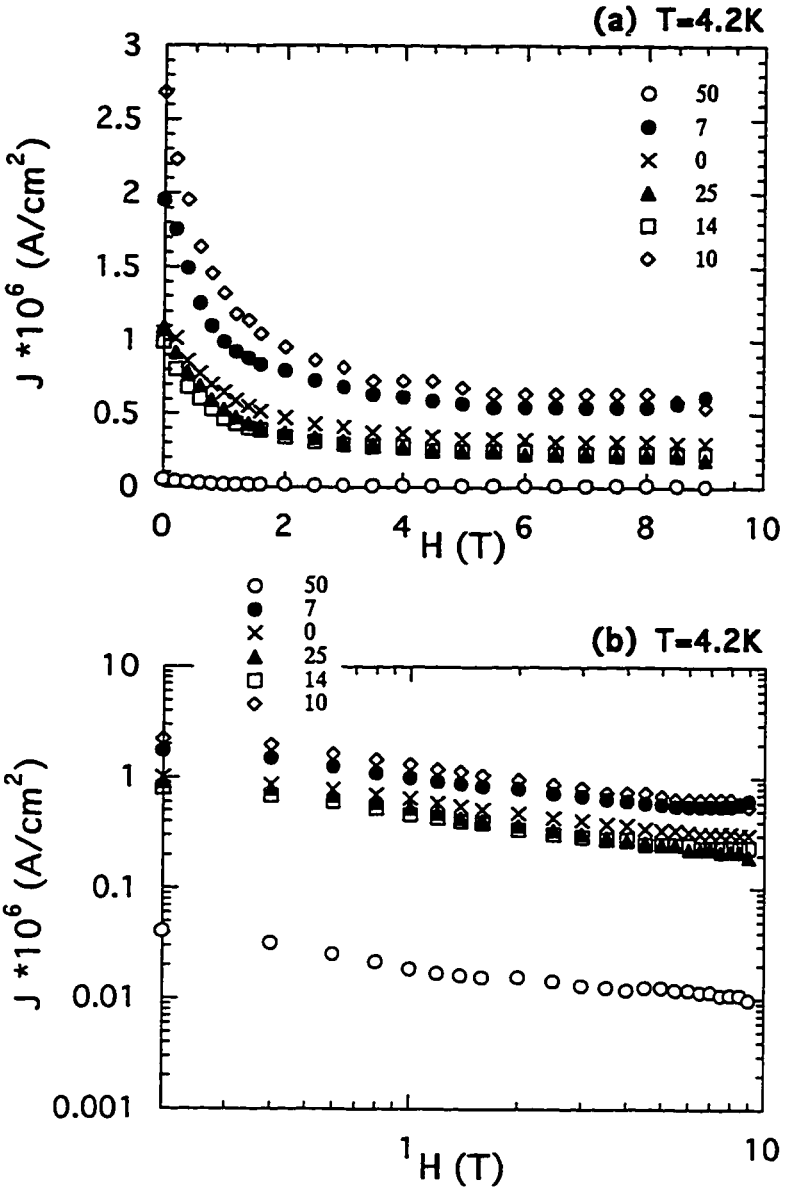

Figure 3.3: (a): Jc(H) curves at different concentrations of Ag2O at T=4.2K.(b): J(H) on log-log scale.

3.3.1 Critical Current Density

Fig(3.3) show the variation of J_c upon changing the applied magnetic field at 4.2K for pure Y_{123} sample. Initially J_c decreases rapidly below applied field of about 2 Tesla, where Jc reaches about half of its value at zero field. This field represents the full penetration field to the sample at 4.2°K. This behavior is followed by very small but gradual decrease in J_c up to the maximum applied field (9T), where $J_c(H = 9T) \approx 0.3J_c(H = 0)$. Figure 3.3 also shows that qualitatively similar behavior is followed for Y_{123}/Ag_2O with different Ag_2O concentration. However, the reduction in the magnitude of J_c at H=2 T is much larger than for pure Y_{123}. For 7% weight ratio of Ag_2O, J_c reduces to about 0.38 J_c(H= 0) and for 10% weight ratio to about 0.33 J_c(H= 0).

At H=9 T, further decrease in J_c for both samples Y_{Ag14} and Y_{Ag10} is observed where, $J_{10}(H = 9) \approx 0.2J_{10}(H = 0)$ and $J_7(H = 9) \approx 0.25J_c(H = 0)$.

Figure 3.3 also reveals that J_c increases as the content of Ag_2O increases up to 10% Ag_2O. However, for higher Ag_2O concentration, the critical current start decreasing, and at above 14% Ag_2O, becomes smaller than J_c of pure Y_{123} following a similar behavior with field, but with a much smaller values than at 4.2°K.

Figure 3.3 clearly indicates that the critical current density follow closely Bean's model at 4.2K and at applied fields larger than the full penetration field(i.e. for $H > 2$ tesla).

3.3.2 Temperature dependance of the critical current

The change in the critical current density in units of Ampere with temperature(Kelvin) gradient is shown in Fig(3.4a,b,c), for pure Y_{123} and Y_{Ag10}. For pure Y_{123}, the critical current drop to about half of its value in the temperature range between 4.2 and 20 K at H=0T. While, at H=2T, the drop is much greater and J_c at 20K has a value of fifth of that at 4.2K reflecting the combined effect of field and temperature on the critical current density. In addition, at H=9T, J_c drops at 20K to about one third of the value at 4.2K.

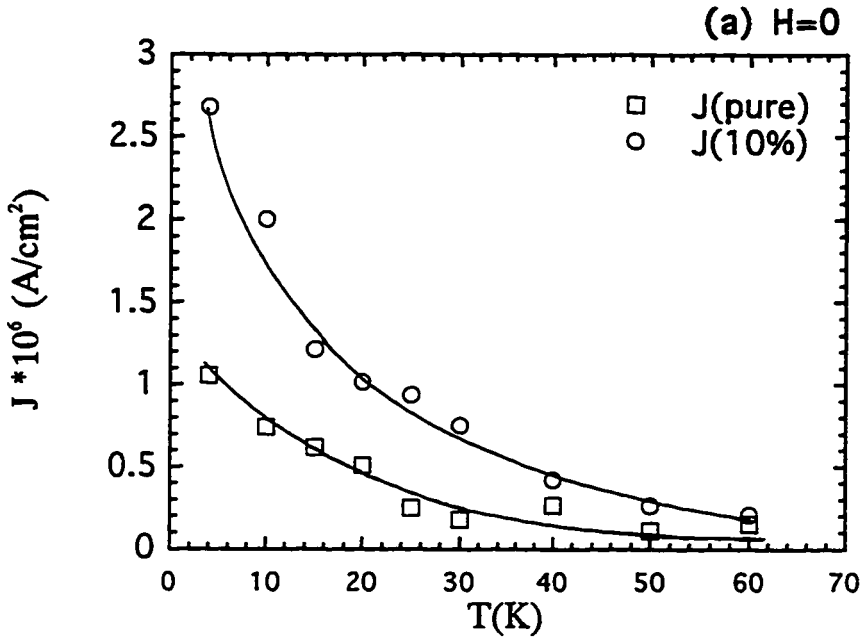
(a) H=0
J(pure)
J(10%)
J *10^6 (A/cm^2)
T(K)
0
0.5
1
1.5
2
2.5
3
0
10
20
30
40
50
60
70

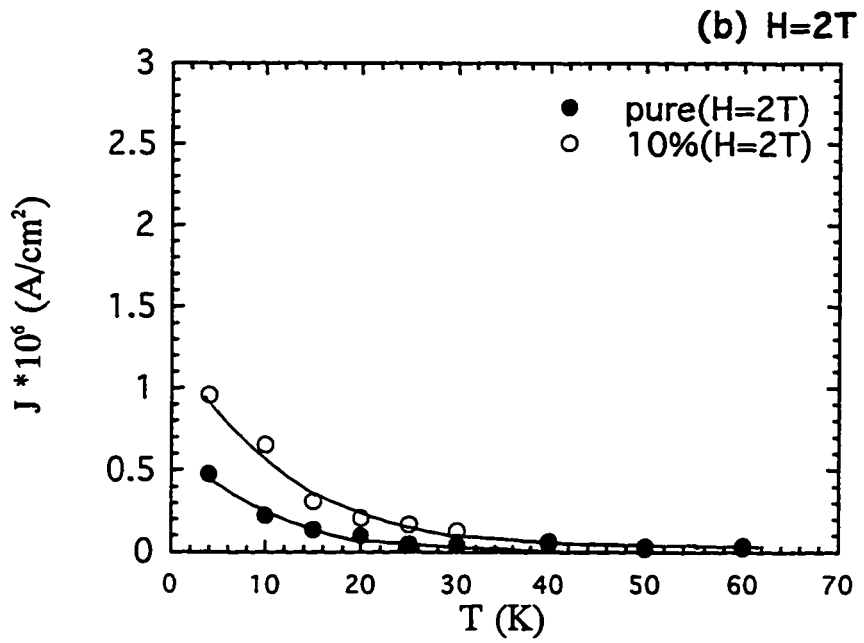
(b) H=2T
pure(H=2T)
10%(H=2T)
J *10^6 (A/cm^2)
T (K)
0
0.5
1
1.5
2
2.5
3
0
10
20
30
40
50
60
70

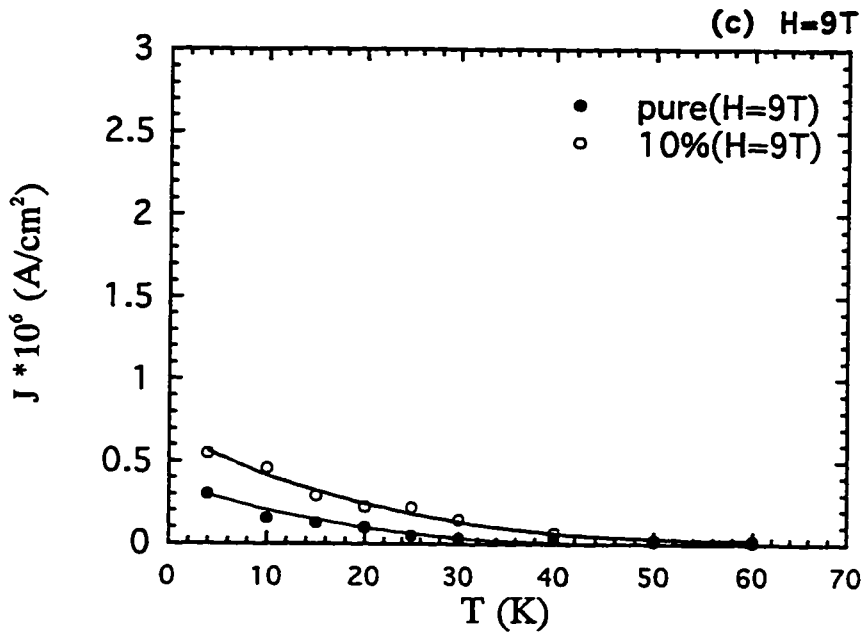

Figure 3.4: a,b,c: Jc(T) curves at Ag2O concentrations of 0% and 10%..

For Y_{Ag10}, the drop in J_c-value for H=2T is similar to that of the pure sample in the same temperature range. For both fields of H=0 and H=9 T, $J(T = 20) \approx 0.33J(T = 4.2)$.

Above 20K up to 60K for all fields, the critical current for both Y_{123} and Y_{Ag10} approximately drop at the same rate and $J(T = 60K) \approx 0.2J(T = 20K)$.

3.4 Pinning Forces

A type-II superconductor can be found in either of three magnetic states. Perfectly superconducting in which the applied magnetic field is below the lower critical value H_{c1}. Normal conductor when $H > H_{c2}$. And a mixed state of normal and superconducting lattice of flux lines in which the applied field has a value between H_{c1} and H_{c2} [1].

The type-II superconductor in a mixed state is "Ideal" if the bulk is free of lattice defects, like(dislocations, grain boundaries, precipitates, etc.). The flux lines (fluxons) of an "ideal" superconductor start to move whenever a force acts on them, and the bulk will go to normal at certain value known as the critical current[4].

Meeting application requirements at temperatures near that of liquid nitro-

gen need high capacity of the superconductor to carry large amounts of critical currents. This is done by introducing pinning centers to the bulk of the superconductor which prevent the flux lines from moving until the pinning force is overcome by the Lorentz force. In our project, the density of pinning centers has been increased and was introduced by adding different weight percentages of silver oxide Ag_2O to Y_{123} HTSC. Experimentally, the pinning force F_p is a function of H, T, and the microstructure of the superconducting sample [39]. In general, the pinning force F_p can be represented as a gradient of a potential function U which carry all the descriptive information and can written as :

$$F_p = -\nabla U \tag{3.4.5}$$

A summary of some theoretical modeling of U has been presented by R. M. Schalk et al. [40]. A simpler way to determine F_p is explained as follows. Since the pinning force is balanced by Lorentz force, its magnitude can be written as :

$$F_p = \left| \vec{J_c} \times \vec{H} \right| \tag{3.4.6}$$

A simple derivation of this equation is given in ref.[10]. Although the critical current density J_c decreases monotonically with field and temperature

(Fig 3.3), the cross product of J and H reveals an interesting features. Fig 3.5 represents the pinning force as a function of the applied field H at 4.2K. For pure Y_{123}, F_p start increasing linearly with field to values of 0.5 T (5000 G). At higher values of field up to 9 T, F_p is still an increasing function of field; indicating that at 4.2K, the maximum pinning force has not been overcome.

The behavior of the pinning forces for Y_{123} above T=30K(as shown in Fig 3.6) reaches a maximum in a field of about 8.5 T then start decreasing after that. At higher temperatures (as can be seen in Fig.3.6), the maximum pinning force occur at a lower values of the applied field. At the maximum temperature in our experiment 60 K, the maximum pinning force occurs at a field of 7.5 T.

3.4.1 The Effects of Adding Ag_2 O on the Pinning Force

The maximum values of the pinning force F_p as well as the distribution of the pinning force is very much affected by the introduction of defects in the superconductor. It has been found that limited Ag_2O addition to Y_{123} compounds provides more pinning centers specially at the grain boundaries, stabilizes the stoichiometry of Y_{123} phase specially the O_2 content [19]. Moreover it has little effect on the orthorhombic crystal structure, and the transition temperature. See Table 1 in chapter 2.

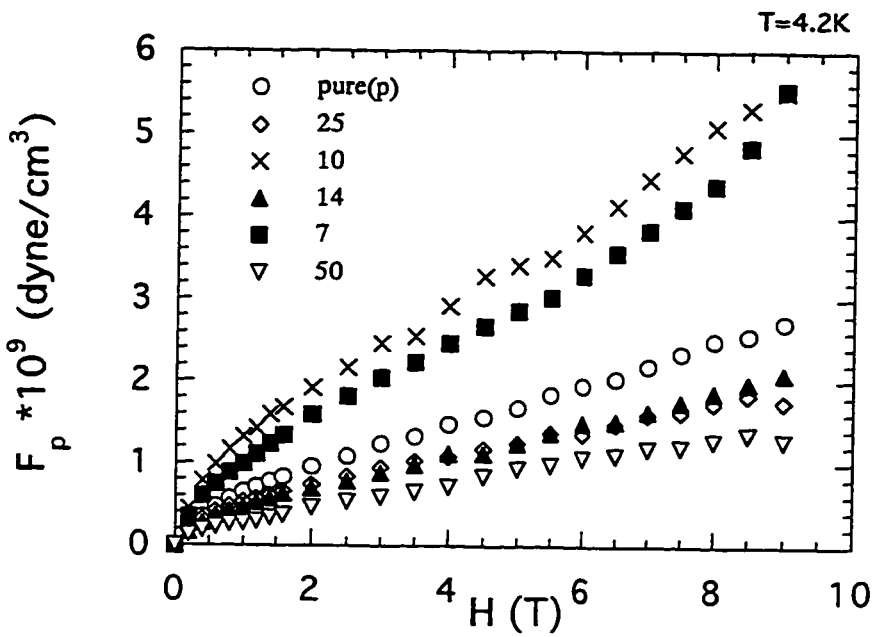

Figure 3.5: Volume pinning force versus field for different contents of Ag2O in Y123 at T=4.2K

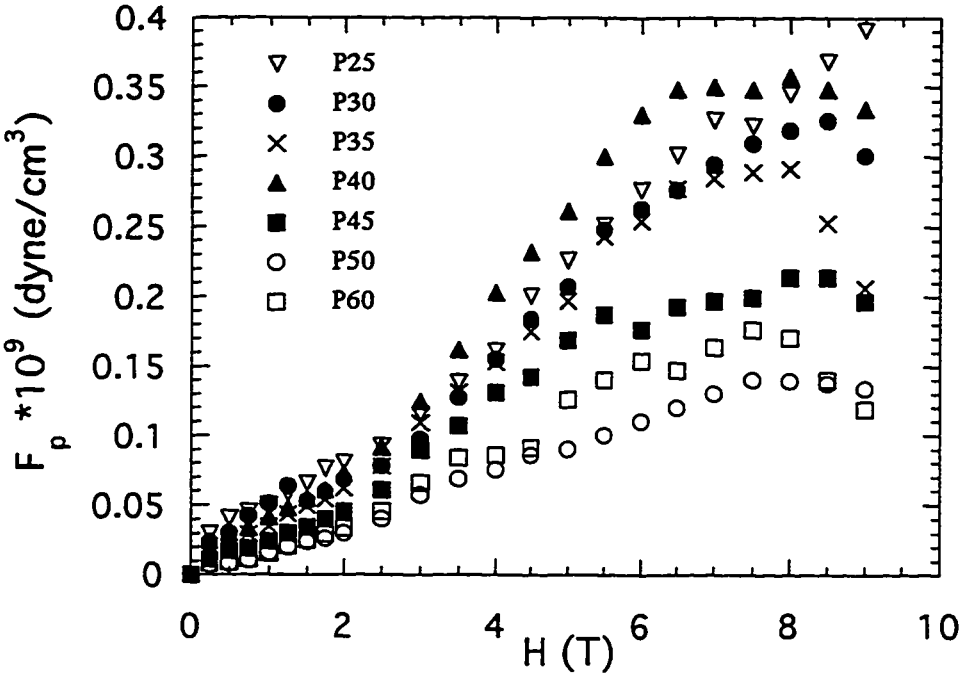

Figure 3.6: Volume pinning force versus field for different temperatures for Y123.

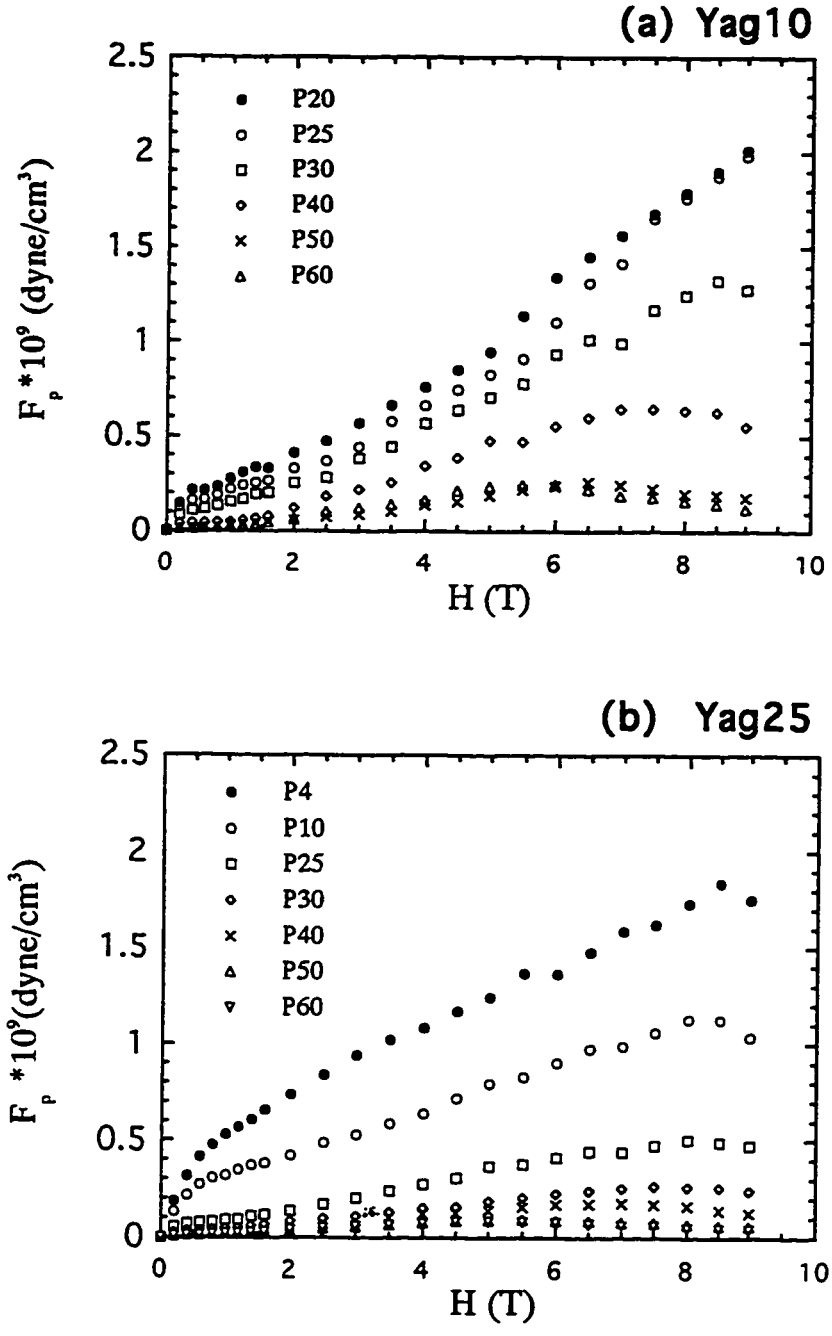

Figure 3.7: a,b: Volume pinning force versus field for different temperatures for YAg10 and YAg25.

Magnetic hysteresis measurements have been carried out on several Y_{123}/ $(Ag_2O)_x$ polycrystalline samples with different Y_{123} : Ag_2O ratios. The magnetization M of all the samples was measured in a field 0-9T, for temperature range between 4.2K and 60K.

The introduction of impurities into the superconductor material may also influence the pinning mechanisms and it may consequently provide a means to control the behavior of the critical current density J_c[41]. In the presence of structural defects (like a percentage of Ag_2O in our case, proton irradiation, neutron irradiation, ...), a position dependance of the free energy of the flux lines arise.

Proton bombardment to superconducting samples, like Y_{123}, create defects (pinning centers) which change the pinning mechanism depending on the energy of the beam.

The pinning force as a function of the magnetic field H is illustrated in Fig.(3.5,3.6,3.7). It is clear that for sample Y_{Ag25} and Y_{Ag50}, the maximum pinning is overcome at 8.5T. In such samples, wt % of Ag_2O reduces the pinning force since it separates the Y_{123} grains. However at 4.2K, even at the maximum value of the applied magnetic field available (9 T), the maximum of F_p is not reached for all other samples. Moreover, one can see that the Y_{Ag10}

has the maximum pinning force through all the other samples in hand.

Magnetic hysteresis measurements at elevated temperatures allow us to determine the temperature, and field dependance of the pinning force. A strong increase of the pinning potential with field has been found at low temperatures, followed by a field dependant maximum and a decrease toward the transition temperature T_c [20].

For Y_{Ag10} as can be seen in fig 3.7-a, two features are observed. First, the maximum pinning force at T=30K has a value of about four times more than that of the pure Y_{123} sample at T=30K. This indicates that the flux pinning is enhanced when the concentration of Ag_2O is increased to 10% percentage weigh relative to Y_{123}. On further increasing the percentage of Ag_2O, the pinning force is found to decrease as can be seen from Fig 3.7-b. In fact, as previously mentioned, the critical current is a maximum at the characteristic percentage of Ag_2O of 10% and it is so for the pinning force which have maximum values for the sample Y_{Ag10}. The data in Fig.3.11. shows that the pinning force (or in other words, critical currents) at 10% Ag_2O percentage weight is largest. It was found by Dwir et al. that the 10% of Ag in Y_{123}/Ag composite samples has the largest critical current [19]. At higher Ag_2O concentration, F_p falls rapidly, probably due to the excess silver which deteriorate the sample and ultimately separate the superconducting grains, thus reducing the intergrain

current carrying .

The second feature which can be revealed from Fig.3.7-a is that the maximum in the values of the pinning force for Y_{10Ag} at T= 60K occur at H = 5.5 T and from Fig.3.7-b (Y_{Ag25}) occur at 4.71 T. The conclusion is that the maximum in the pinning force occur at a smaller values of H upon increasing the temperature or the percentage of Ag_2O. To be able to see exactly the consequences of adding Ag_2O to Y_{123}, the curves (F_p vs H) of each sample must be discussed in terms of scaling arguments which we will be presenting in the following section.

In Fig.3.8., for Y_{Ag14}, the volume pinning force is presented as a function of field and temperature. It can be seen that F_p has peak at values of the applied field H that decrease as the temperature increase.

3.5 Scaling Behavior of The Pinning Force

Scaling law was first introduced by Fiets and Webb in 1969 for a phenomenological description of experimental results on cold-worked Nb-based alloys [10].

The recognition of scaling laws are useful for two reasons. First, it can predict the value of the pinning force at any temperature once it is measured at one single temperature. Second, a plot of F_p versus the reduced field (b) can

give a lot of qualitative information about the pinning mechanism and about the distribution in the pinning force [10].

A complete picture of the pinning force in different samples of Y_{123} / $(Ag_2O)_x$ can be explained qualitatively through the scaling analyses. Referring to fig(3.8), where the pinning force F_p vs H is plotted for Y_{Ag14} at different temperatures and F_p is calculated from equation 3.4.6. At a given temperature F_p is zero at $H = 0$ and at $H = H_{c2}$ (upper critical field), reaching a maximum value F_{max} at some intermediate field H^* [20]. Both of these values F_{max} and H^* decreases with increasing temperatures. In general, at a given field F_p and F_{max} have the same temperature dependance, then the ratio $\frac{F_p}{F_{max}}$ is temperature independent.. Similarly, at a given temperature $\frac{F_p}{F_{max}}$ will be field independent if represented as a function of $\frac{H}{H^*}$ [20].

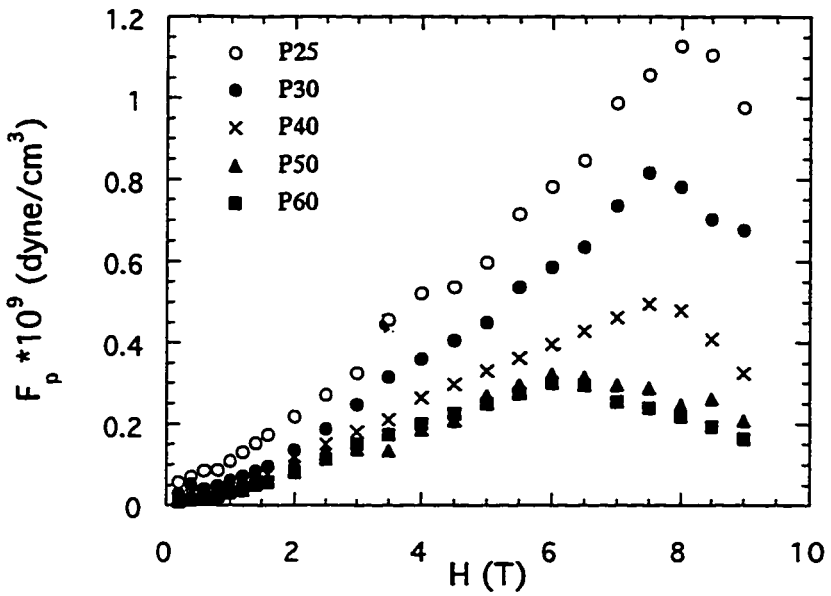

Figure 3.8: Volume pinning force versus field for different temperatures for YAg14.

Scaling behavior suggest that all F_p(H,T) curves measured at different fields and temperatures can be superimposed in a single curve of F_p/F_{max} versus the reduced field H/H^* that have a maximum at a normalized values of the pinning force and applied magnetic field [20]. In conventional superconductors, scaling behavior is found for F_p/F_{max} vs H/H_{c2} [10]. However, H_{c2} is very high (about 200 T at 4.2K) in Y_{123}/Ag_2O HTSC, and can be replaced by H^*or H_{irr} if they have similar temperature dependance. The irreversibility field H_{irr} is the field at which the pinning force vanishes, where the width of the hysteresis loop becomes zero [41], and H^* is the field at which $F_p = F_{max}$. The scaling analysis for Y123 and Y_{123} / $(Ag_2O)_x$ is presented in Fig 3.9(a-f) in which the normalized force is expressed as p=$\frac{F_p}{F_{max}}$ and the normalized field as h=$\frac{H}{H^*}$

The scaled (normalized) curves are shown in Fig 3.9 from which we can see that for Y_{123} sample and Y_{123} / (Ag_2O) samples with Ag_2O concentrations less than 25%, the figure exhibit an initial upward increase in the pinning force at low fields. Similar upturn behavior was recorded for proton-irradiated Y_{123} samples by Thomson and Christen for a density of (3×10^{15} ions/cm^2–8×10^{16} ions/cm^2) [20]. In this case J_c initially increases with H, (the so called peak effect which is due to fishtail effect) and so that F_p (J, H) increases faster than linearly. In contrast as the density of defects increases, as in samples

(25% and 50%), J_c decreases monotonically with H and the upward curvature in F_p is absent , This is also has been seen in proton-irradiated Y_{123} samples with high density of defects [20].

The scaling is observed for the doped and undoped samples. At any level of doping with silver, the scaling procedure made all curves of F vs H to fall into a single curve F/F_{max} vs H/H_{max}. The existence of the scaling behavior of F_p that describes the data for the temperature range of our experiment (4-60K) suggests that J_c is determined by a single type of pinning center[20].

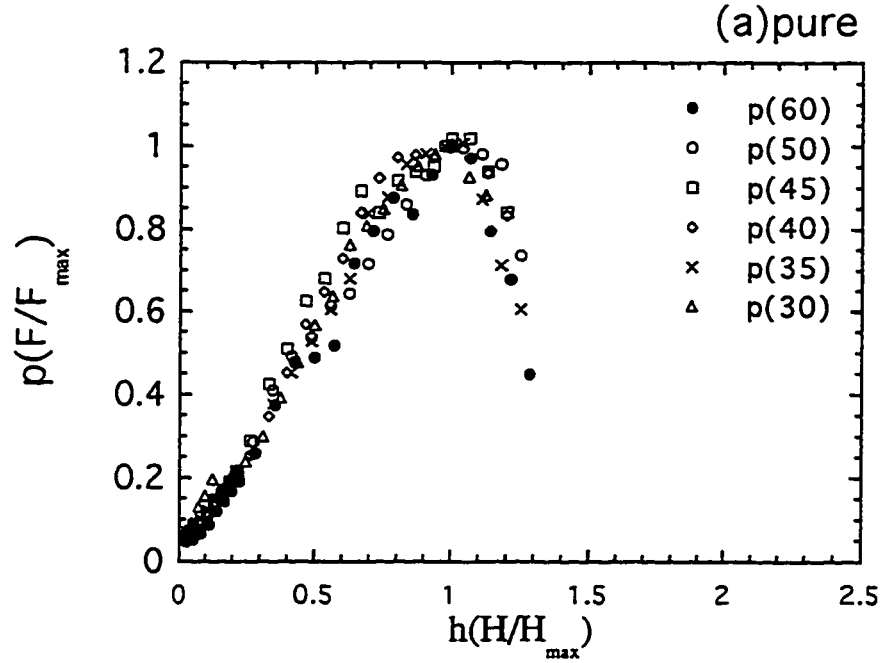
(a)pure
p(60)
p(50)
p(45)
p(40)
p(35)
p(30)
p(F/F max)
h(H/H max)
0
0.2
0.4
0.6
0.8
1
1.2
0.5
1.5
2
2.5

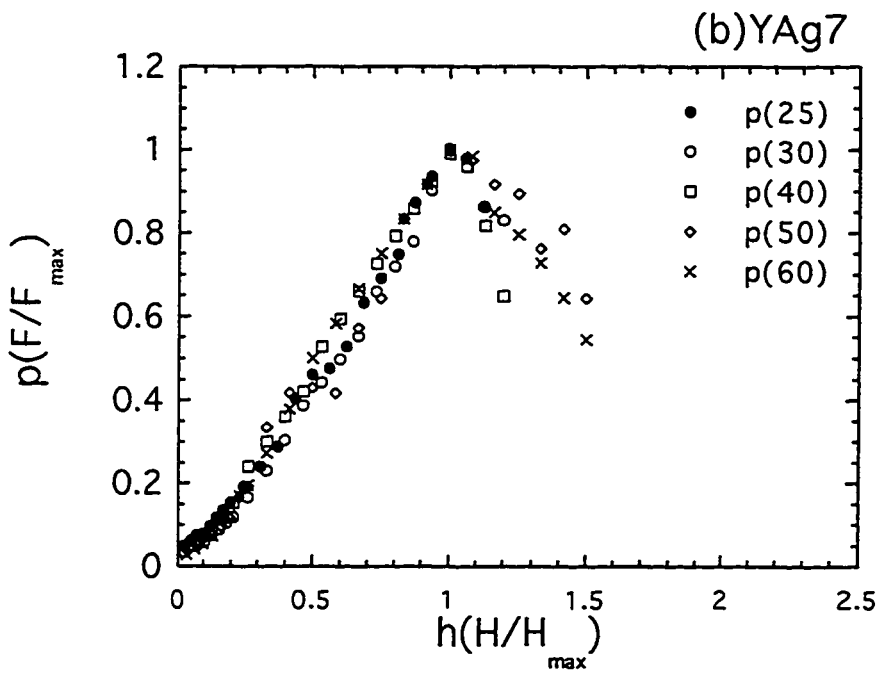
(b)YAg7
p(25)
p(30)
p(40)
p(50)
p(60)
p(F/F max)
h(H/H max)
0
0.2
0.4
0.6
0.8
1
1.2
0.5
1.5
2
2.5

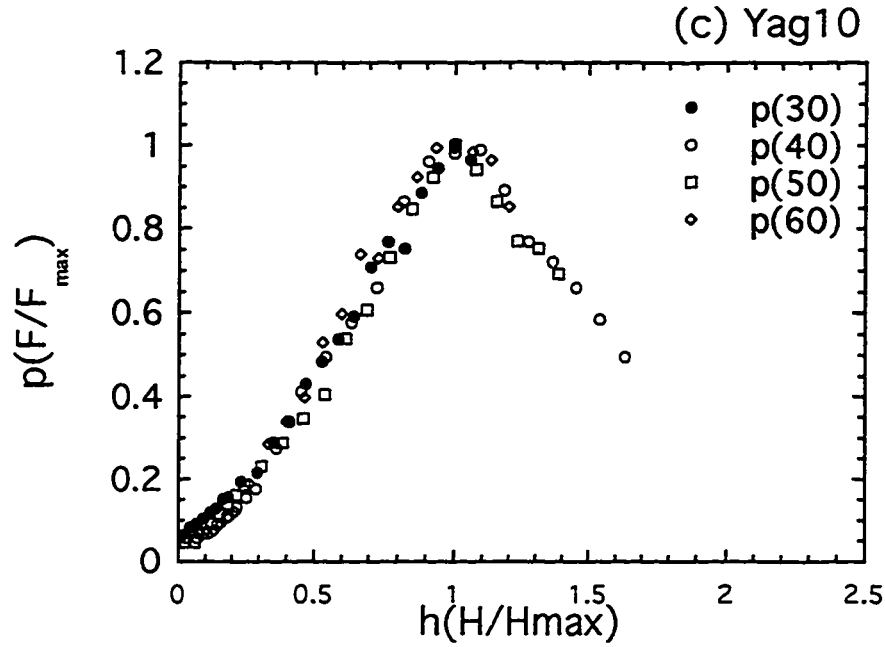
(c) Yag10
p(30)
p(40)
p(50)
p(60)
p(F/F max)
h(H/Hmax)
0
0.2
0.4
0.6
0.8
1
1.2
0.5
1.5
2
2.5

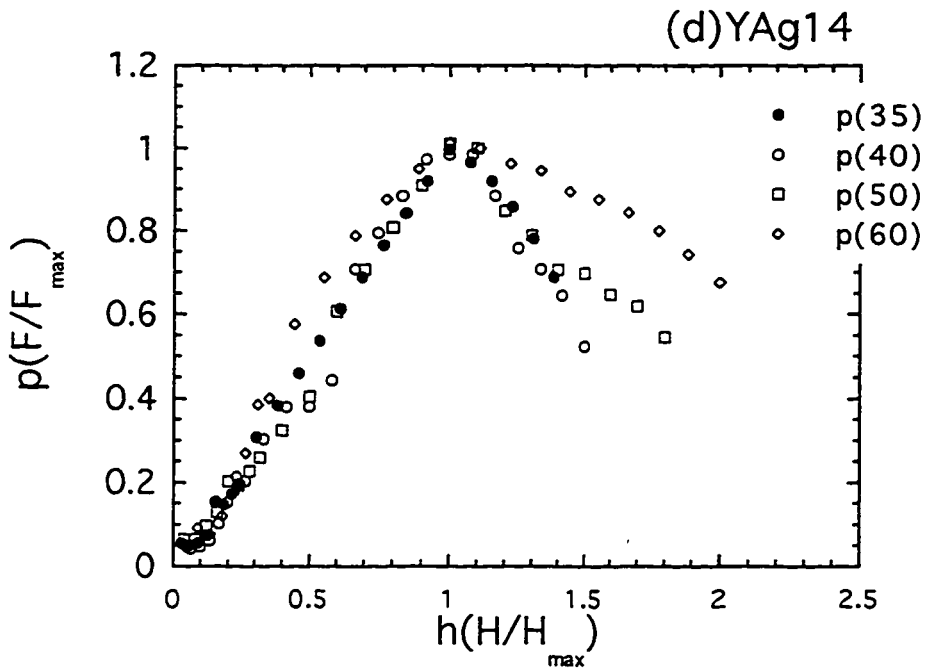
(d)YAg14
p(35)
p(40)
p(50)
p(60)
p(F/F max)
h(H/H max)
0
0.2
0.4
0.6
0.8
1
1.2
0.5
1.5
2
2.5

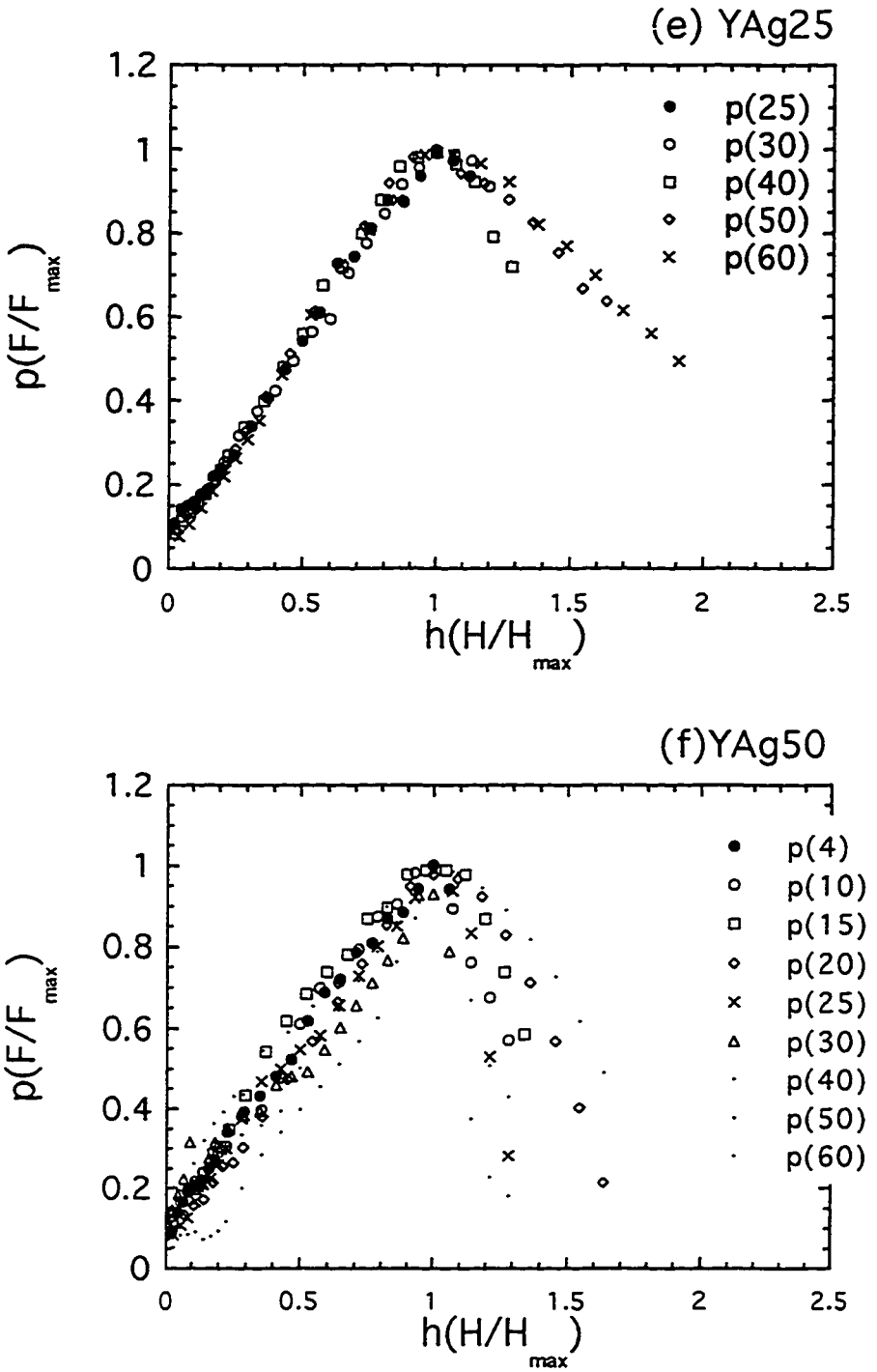

Figure 3.9: a,b,c,d,e,f : Normalized volume pinning force versus reduced field for different temperatures.

The pinning force curves obey a general form

$$Fp = \alpha \cdot H_{c2}^{n} \cdot f(b) \tag{3.5.7}$$

where $b = H/H_{max}$, α, n are constants and $f(b)$ is a function only of the reduced field b [10].

Referring to Fig.3.10, at the maximum field of 9T, the pinning force is not overcome until the temperature exceeds 25K for all sample other than Y_{Ag50}. As the temperature increases, the thermal energy available increases the possibility of the vortices to jump the pinning potential barrier.

For the deteriorated Y_{Ag50} sample, the maximum pinning forces is overcome at very low temperature (8K) compared to other samples in hand in which the F_p has not yet been reached at temperature less than 25K. The maximum field H_{max} needed to overcome the maximum pinning force at T= 30K is presented in Fig. 3.12 as a function of the weight ratio silver oxide content. The maximum value of H_{max} occurs at $x \approx 10\%$, consistent with results obtained from the maximum critical current density. This reflects the strong pinning mechanism controlling the motion of the flux lines of Y_{10Ag}. Moreover, the pinning force is very weak for $x > 15\%$ compared to values for $x < 15\%$.

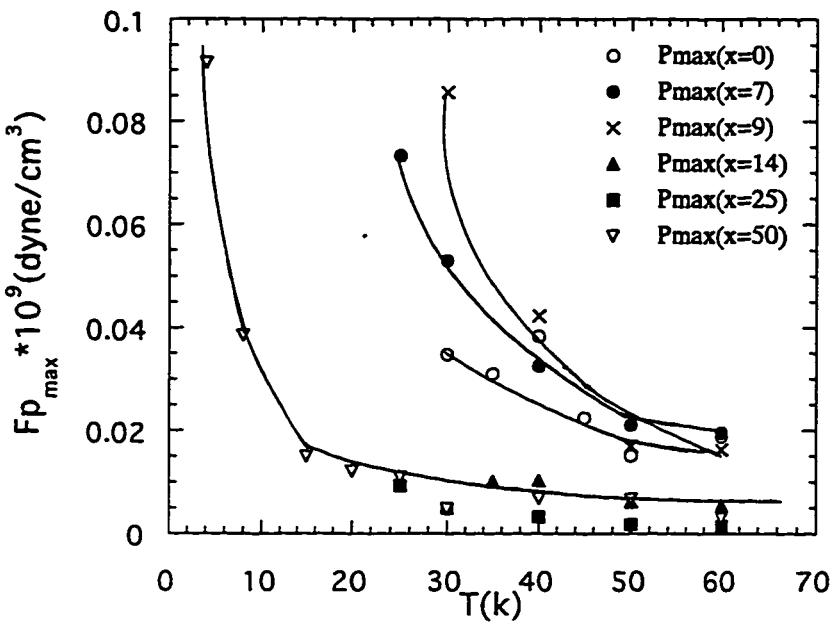

Figure 3.10: The maximum pinning force versus temperature for different samples of Y123/(Ag2O)x

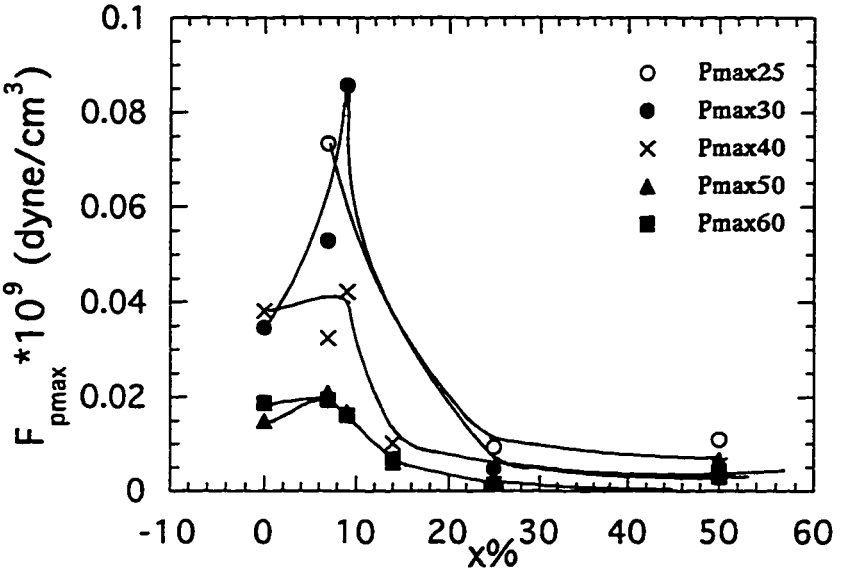

Figure 3.11: The maximum pinning force versus concentrations for different temperatures

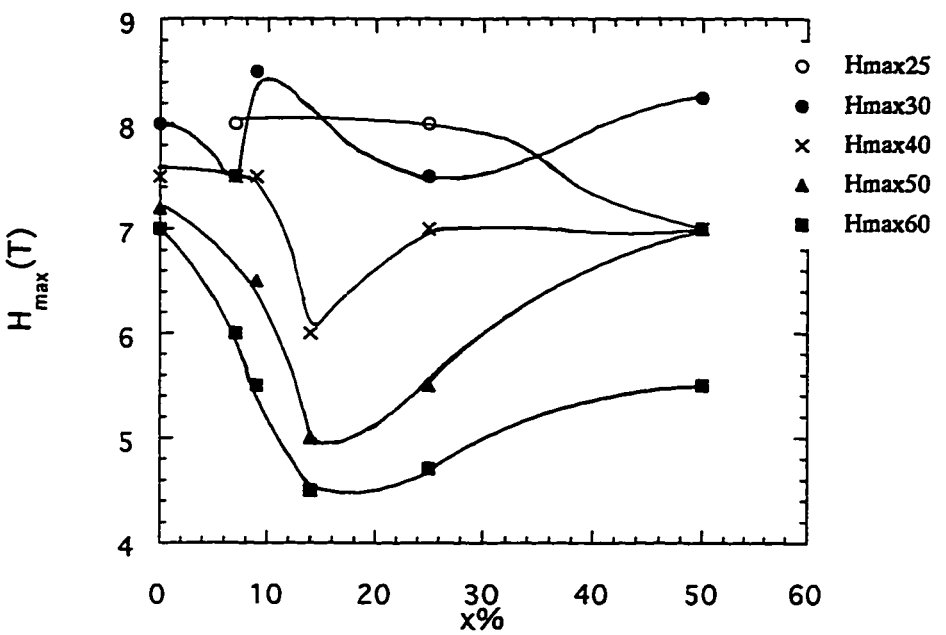

Figure 3.12: The maximum field versus concentrations for different temperatures

Close inspection of Fig.3.9a-f for Y_{123} and $Y_{123}/(Ag_2O)_x$ with different Ag_2O contents, one can deduce some consequences of Ag_2O addition to Y_{123}.

It is clear that for pure sample Y_{123}, the distribution of the pinning force occur at a narrow range of the reduced field b(Fig 3.9a), while this range is broaden for silver containing samples such as Y_{25ag}(Fig 3.9e). This is directly related to the behavior of the pinning force as the number of defects increase. In other words, the pinning force change abruptly around the maximum with fields for samples of weight percent of Ag_2O below 10%. in pure samples abruptly, while it goes gradually to its maximum (relax) in doped samples.

The behavior of F_p as a function of the reduced field b is described in equation 3.5.7 to be

$$Fp = \alpha \cdot H_{c2}^{n} \cdot f(b) \tag{3.5.8}$$

since H_{c2} and H_{max} have the same temperature dependance [41], we can without loss of generality replace H_{c2} by H_{max} and write[53]:

$$Fp = \alpha \cdot H_{\max}^{n} \cdot b^{\frac{1}{2}}(1-b)^2 \tag{3.5.9}$$

To find n , the logarithm of F_{pmax} is plotted versus the logarithm of H_{max}

for different Y_{123}/ Ag_2O samples . With the best fit, the value of n is given in Table 3.1 where it is found that for pure sample n is 1.43. However, for Y_{Ag7} and Y_{Ag10} it has values of 2.1 and 2.34 respectively. For the samples with Ag_2O percentage of mare than 10%, n has a low values as shown in the table. The values for Y_{Ag7} and Y_{Ag10} are in complete agreement with that of the system in which the transition elements (Fe, Co, and Ni) are doped in Y-Ba-Cu-O[41].Moreover, a value of n=2.56 was obtained by C.D. Wei et al. for pure Y_{123} system[53]. For pure neutron irradiated Y_{123} crystal system, since obeying the general Fietz-Webb universal scalling law is a strong evidence that flux pinning is the mechanism which determines J_c, the high value of n=2.56 indicates that this irradiated system has higher pinning forces at high fields and more defects which cause it to have higher J_c than non-irradiated samples.

We have shown that the pinning forces for the doped and undoped samples obey a scaling law over the whole range of temperature and field accessible in our system with the exception explained before for Y_{Ag50}.

Table 3.1: Results of the best fit of the pinning force Fp where n is evaluated and has a larger value for 10 percent of Ag content indicating that Fp is largest in this sample among all of the samples under the scope.

sample	n
Y123	1.43
Y7ag	2.1
Y10ag	2.34
Y14ag	0.3
Y25ag	0.19
Y50ag	0.07

Chapter 4

Energy Loss

4.1 Introduction

Energy loss characteristics of the cuprates (high-temperature superconductors) are of particular interest since these materials are proposed to be used in power transmission and generation. The seemingly impossible demand to obtain a perfect superconductor "ideal" that carry high critical currents at elevated (LN2) temperature demands a closer look to the details of the intricate nature of the magnetic state of HTSC.

Energy losses in type-II superconductors are mainly due to the irreversible motion of the magnetic fluxons due to their interaction with pinning sites [42, 43, 44, 45]. However, energy loss due to eddy currents in the normal

fluxoid cores may also contribute to the total energy losses depending on the geometry of the superconducting sample [46].

Energy losses can be categorized as transport and magnetic energy losses. In transport measurements (AC and DC), energy is being lost in the form of Joule heating (namely IV). Magnetic energy losses is due to the work done by the external field that produce changes in the magnetization of the superconducting material i.e. that generates changes in the density of the trapped flux. This is also dissipated as heat inside the superconducting material.

So far, most of the research that has been conducted on the energy losses in HTSC are performed in the presence of AC transport or AC-magnetic field, with different frequencies. However, it was found that at low frequencies ($\sim$60 Hz), magnetic and transport energy loss are approximately the same [47].

Another source of losses is the vortex annihilation in which the moving vortices of opposite magnetic field direction can annihilate [42]. Other sources of dissipation are discussed by Kadowaki et al.[48]. In this chapter we will be considering magnetic energy losses produced by cycling the applied magnetic field for polycrystalline Y_{123} and $Y_{123}/(Ag_2O)_x$. However, for single crystalline samples, the crystalline anisotropy may affect the magnitude and the mechanism of the energy loss [46].

4.2 Magnetic Energy

The energy dissipated in a superconductor due to a cycling magnetic field is simply obtained by evaluating the area of the hysteresis loop [49, 50, 51]:

$$W = \oint MdH \tag{4.2.1}$$

where M is the magnetization of the superconducting sample and H is the applied DC or AC magnetic field.

In hysteresis loops, the contribution to magnetization is coming from diamagnetism plus trapped flux moments, consequently the total energy dissipation source is either the diamagnetic or the trapped flux contributions. In magnetic measurements, below H_{c1}, minimal energy loss is observed(very little hysteresis). However, when the field applied exceeds the critical lower value H_{c1}, hysteresis is created and energy dissipation accumulates.

From the hysteresis loops of Figures 3.1and 3.2 for Y_{123} at 4.2K, one can see three different energy loss states. For low fields lower than H_{c1}, the loss is very small where the hysteresis losses are minimal, the magnetization is almost reversible. The loss in this region is called the intergranular loss in which the small magnetic field penetrate easily the weakly coupled Josephson junctions formed between the superconducting grains [51]. For fields that exceeds H_{c1}

but less than the full penetration field H_p (which is $\sim$ 2 Tesla in this case), it was predicted by Bean[37] that the energy loss approximately exhibit a field dependance of $W \propto H^3$. In this region, the losses are mainly caused by bulk pinning losses in which a moderate magnetic fields penetrate the grains in the form of Abrikosov-like vortices (intra-granular losses) [44, 51]. The total hysteretic losses in HTSC is then the sum of the intergranular and intragranular losses [51].

As the applied field increase above H_p Bean have predicted that the energy loss is nearly proportional to the amplitude of the applied magnetic field H. In general, a power law with different exponents describes the dependance of the energy loss on the applied magnetic field. Similar results have been found for $REBa_2Cu_3O$ by Yunhui Xu et al. (RE=Gd, Dy, Er, Eu, Y)[43]. Yunhui et al. have found that for $GdBa_2Cu_3O_7$ at T=4.2K and very small fields of few gauss, the AC-losses vary with the seventh power of the amplitude of the applied field H_o(47).

In this project, we are going to study the energy losses in HTSC Y_{123} and the composite Y_{123}/Ag_2O generated by a DC applied magnetic field.

4.3 Results and Discussions

4.3.1 Field Dependance of the Energy Losses

For different concentrations of silver oxide ranging between 0% and 50% have been added to pure Y_{123}, the energy loss is studied as a function of amplitude of the cycling applied magnetic field. The energy dissipated for all of our samples at 4.2K is plotted against the magnitude of the cycling field H (log-log scale) as in Fig (4.1). The magnetic energy losses are calculated by numerically evaluating the area of the hysteresis loops shown in Fig 3.1,3.2 and other hysteresis loops at a fixed temperature but with different cycling fields.

Figure 4.1 shows that at high values of H, the energy loss approaches saturation at a field which is much larger than the full penetration of the magnetic field in the superconducting sample [43, 51, 52]. On the other hand, at low fields, a stronger field dependance is followed.

The relation between the energy loss W and the applied field H follows a power low as :

$$W \propto H^n \tag{4.3.2}$$

which becomes linear on log-log scale(log W$\propto$n log H)

According to the behavior of W for different regions, the power of H at low

fields will be denoted as n_1 and that for high fields as n_2

For pure Y_{123} and low field, the exponent n_1 ~1.39, and the high field, n_2 is about unity

For samples that have silver (Table 4.1), it is found that as silver is added, n_1 increasing to a maximum value at 10% of Ag_2O. For Y_{Ag2}(50 % of Ag_2O) the energy loss is proportional to $H^{0.65}$ which is stronger field dependance than that of Y_{Ag7} and Y_{Ag4} but has a smaller values of W. The n_2 at high fields, with best fitting, is unity which indicates a good agreement with Bean's model.

We have found in the previous chapter that the critical current and the pinning forces are maximum at 10% concentration of silver. This indicates for $Y/(Ag_2O)_x$ with 10:1 weight ratio that higher losses are related to wider hysteresis loops, higher pinning forces and higher critical current densities and stronger energy-field dependance [51]. The values of n_1 and n_2 for the other samples are presented in Table 4.1.

In comparison with Bean's model, the result for high values of H are in excellent agreement and shows linear behavior above the full penetration field. n_1 is expected according to Bean's Model to be 3, however, at low fields as it is clear from Table 4.1, where its values range between 0.65 and 2.41 showing a disagreement with Bean's Model.

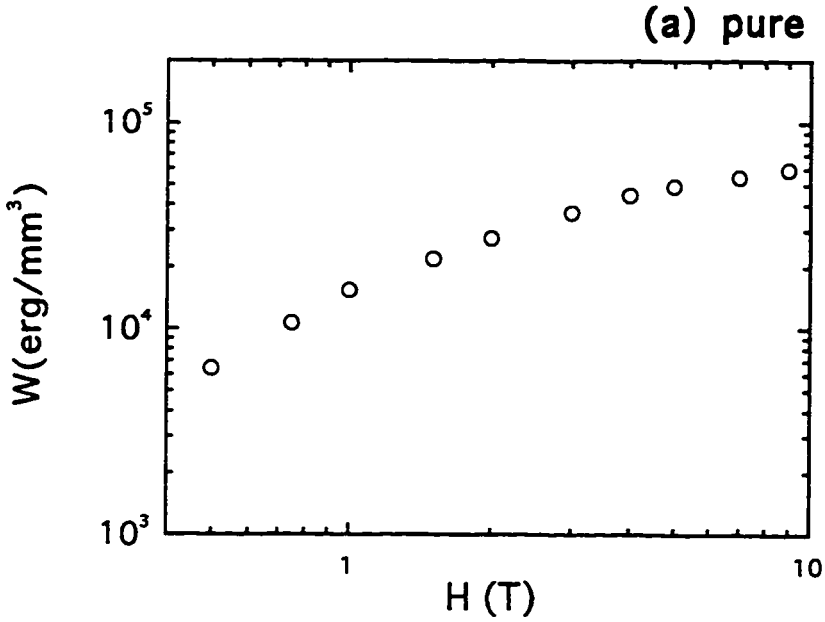
(a) pure
W(erg/mm^3)
10^5
10^4
10^3
1
10
H (T)

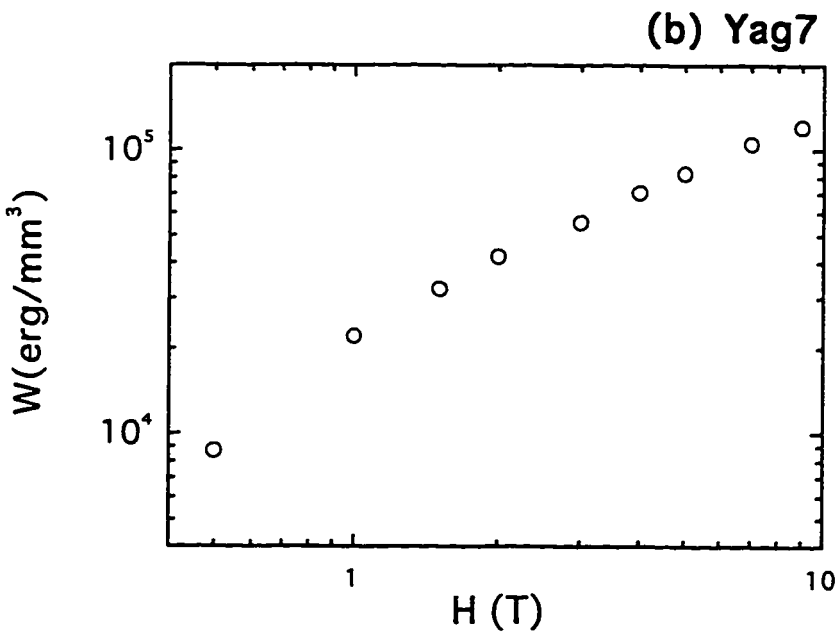
(b) Yag7
W(erg/mm^3)
10^5
10^4
1
10
H (T)

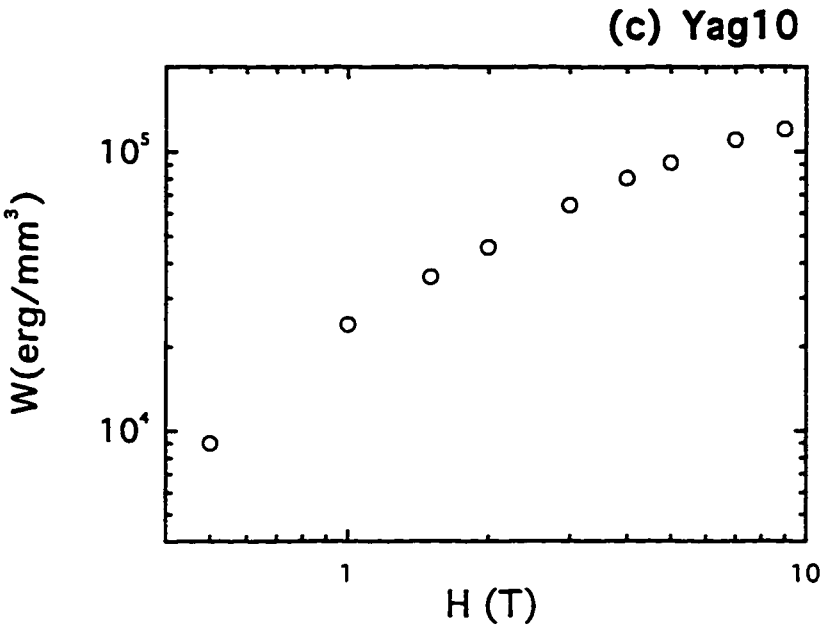
(c) Yag10
W(erg/mm³)
10⁵
10⁴
1
10
H (T)

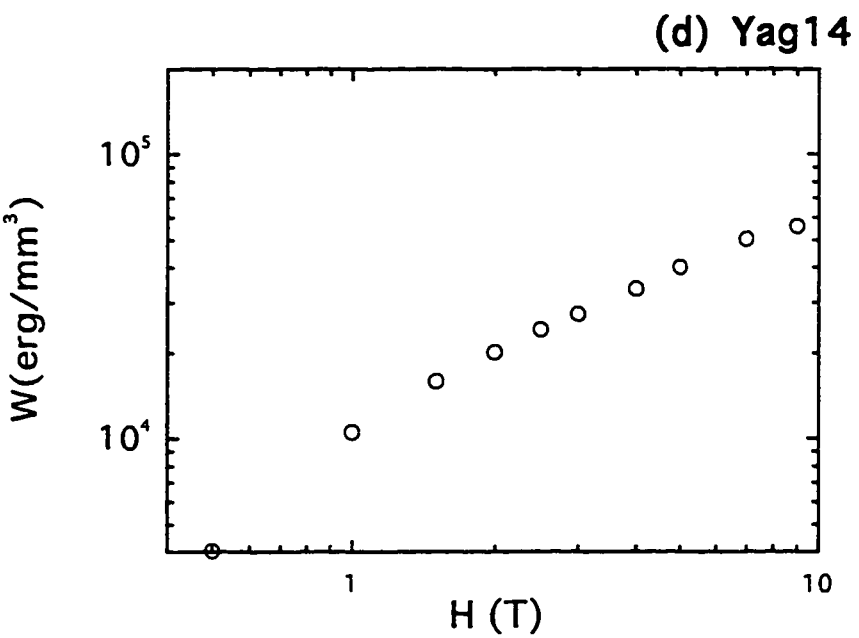
(d) Yag14
W(erg/mm³)
10⁵
10⁴
1
10
H (T)

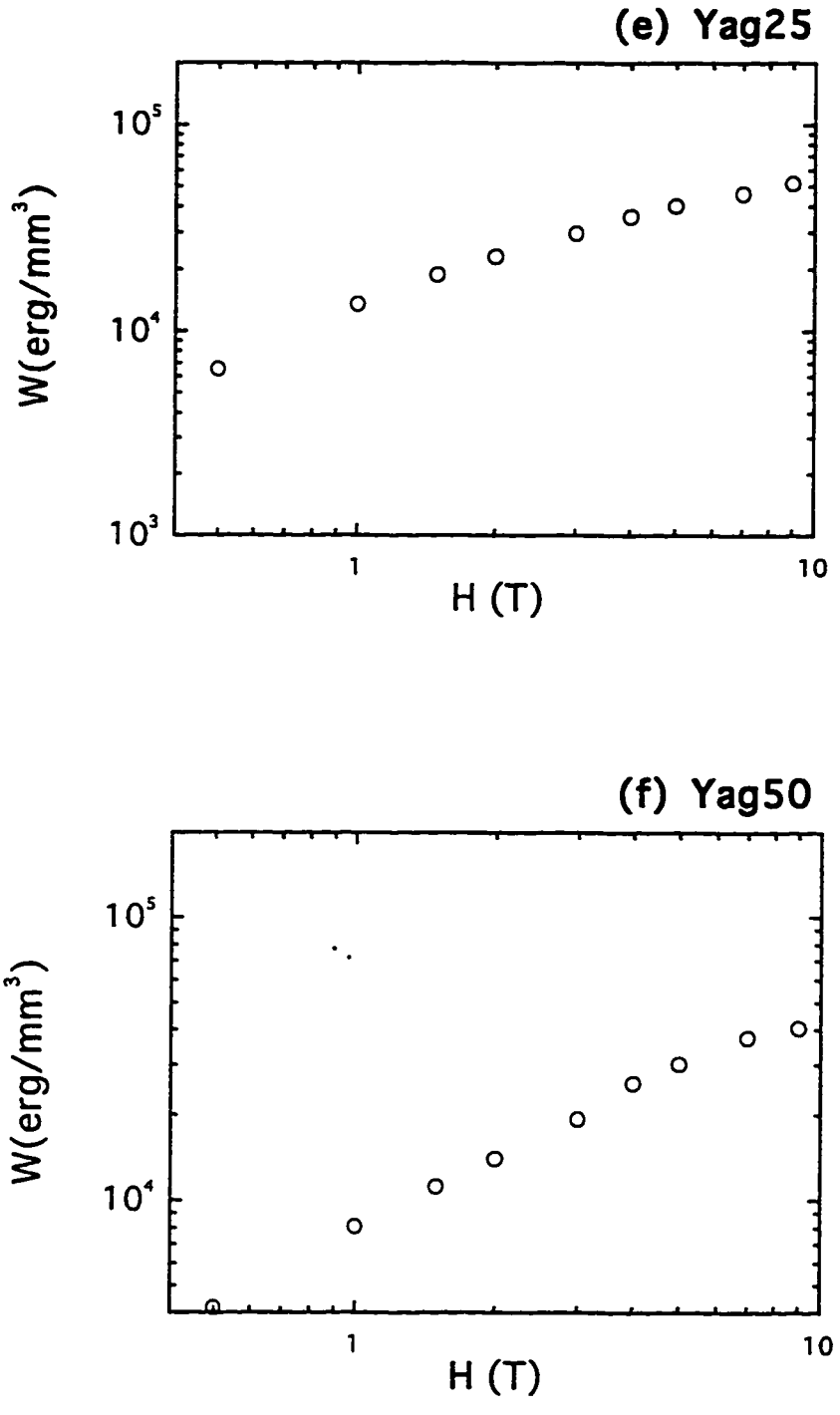

Figure 4.1: a,b,c,d,e,f: Total energy loss versus field at T=4.2K

Energy loss dependence on H has been found to change depending on the rare earth present in HTSC i.e. $REBa_2Cu3O_7$. For example, Yunhui Xu et al have shown a consistent result with Bean's for $REBa_2Cu3O_7$ (where n$\sim$3 for $H < H_p$ and n$\sim$1 for $H > H_p$). However, for Y_{123} single crystal, deviations from Bean's model can be seen in the work of Kh.A.Ziq et al [51]. Furthermore, the changes in the exponent n has been also investigated as the oxygen content is slightly varied in $Y_1Ba_2Cu_3O_x$ and some deviations are presented in ref. [52]. Astra found that the maximum exponent of 1.92 occur at x=6.9 [52].

4.3.2 Temperature Dependence of the Energy Loss

The hysteresis loops shown in fig 3.1 and 3.2 for Y_{123} HTSC at different temperature and for cycling between $\pm$90kOe. The loops are symmetric around the origin. In the first and third quarters, the magnetization M is along the same direction of H which indicates that the superconductor has a paramagnetic component and is mainly due to the trapped magnetic flux. However, in the second and fourth quarters the sample is diamagnetic, the negative magnetic moment is due to the supercurrent circulating the sample. As explained previously, the area under the M-H loop is the energy loss, so the energy dissipated due to the creation of the trapped flux lines is the sum of the areas of the

first and the third quarters. Similarly, the diamagnetic response of the energy loss W_{dia} is the sum of the areas of the second and fourth quarters. The total magnetic energy loss W is the sum of the diamagnetic and the trapped flux contribution to the energy. Figure 3.1 indicates that the area(energy loss) decrease as the temperature increase. The variations of the magnetic energy loss with temperature can be seen more clearly in Fig. 4.2 which is presented on a semi-log scale for Y_{123}. The figures reveals that W is inversely proportional to T, i.e. W decreases exponentially with T ;we have;

$$W = W_0 e^{-\beta T}$$

where W_0 is the value of the energy loss extrapolated at T=0, and β is a constant [43].

Similarly, the energy associated with the creation of trapped flux W_{trap} and that due to the diamagnetism of the sample W_{dia} is also presented in Fig 4.2. Initially, at low temperature W_{trap} decrease with a slope that is about double that of the diamagnetic loss. This means that initially the flux lines are leaving the sample at a high rate. However, at higher temperatures (> 20 for Y_{123}) the slope of the trapped energy decrease becoming approximately equals the slope of the diamagnetic loss i.e. both decrease with temperature with the same rate.

The best linear fit for the trapped flux energy loss gives $W_0 = 7.27 \times 10^5$ erg/cm^3 and $\beta = 0.188$. For the total energy, however, $W_0 = 8.2 \times 10^6$ erg/cm^3 and $\beta = 0.038$. The diamagnetic contribution W_{dia} is almost parallel to W_0 and has nearly the same $\beta(.036K^{-1})$ as can be seen from Table 4.2. Also, we can see from Fig.4.2 that the energy of the trapped flux is consistently smaller than that of the diamagnetic,(W_{dia}=5.32×10^6erg/cm^3 at $T = 0$ extrapolated).

For other that contains silver oxide samples we have the results are presented in Fig 4.2b-f, W_{trap} extrapolates to zero at a temperature T_{trap} ranging between 30K and 40K. As W approaches zero, the flux lines are more free to move [50]. The values of W_0 and β for the other samples are presented in Table 4.2. W is maximum for Y_{Ag10} among all samples we have. The loss is minimum in the deteriorated samples of Y_{Ag25} and Y_{Ag50}.

In comparison for Y_{123} with the work of Yunhui Xu et al. for $GdBa_2Cu_3O_7$, they found that the total energy loss $W_0 = 1.07 \times 10^5$ erg/cm^3 which is an order of magnitude lower than that of our project Y_{123}. However, they had a value for β which is in good agreement with what we found ($\beta = 0.05$). Furthermore, for Bi(2223), Kh. A. Ziq et al. had the same order of magnitude for the energy loss ($W_0 = 3.369 \times 10^6$ erg/cm^3). The energy loss is maximum when silver is added to Y_{123} with a concentration of 10%.

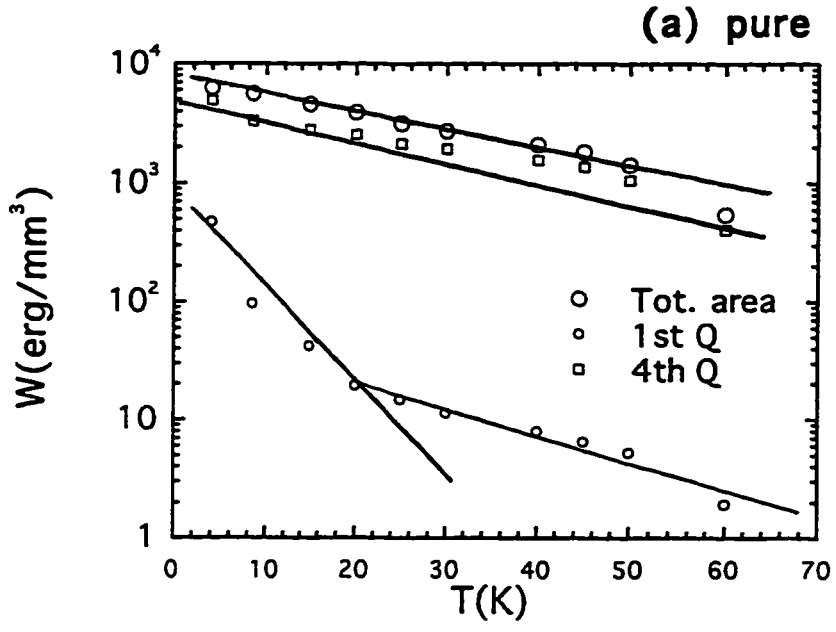
(a) pure
W(erg/mm³)
T(K)
Tot. area
1st Q
4th Q

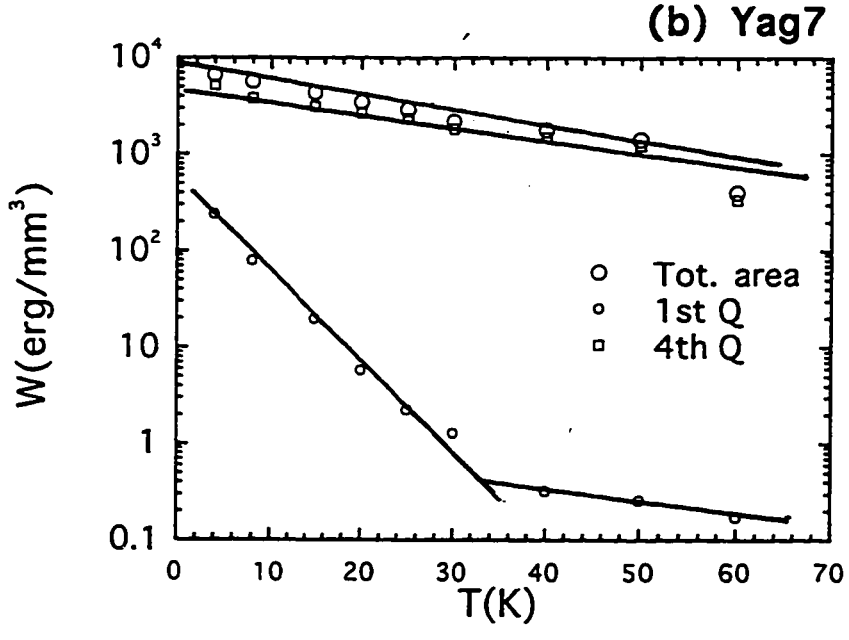
(b) Yag7
W(erg/mm³)
T(K)
Tot. area
1st Q
4th Q

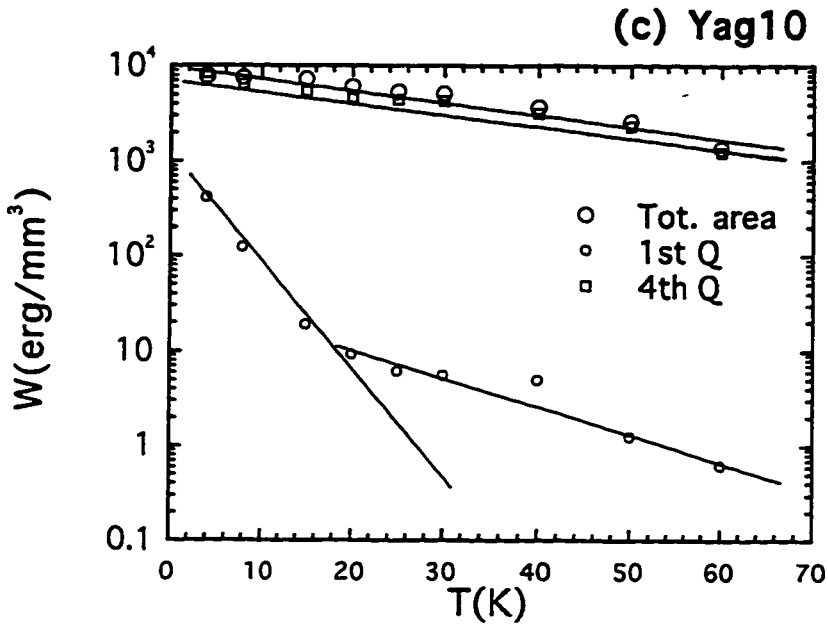
(c) Yag10
W(erg/mm^3)
10^4
10^3
10^2
10
1
0.1
0
10
20
30
40
50
60
70
T(K)
Tot. area
1st Q
4th Q

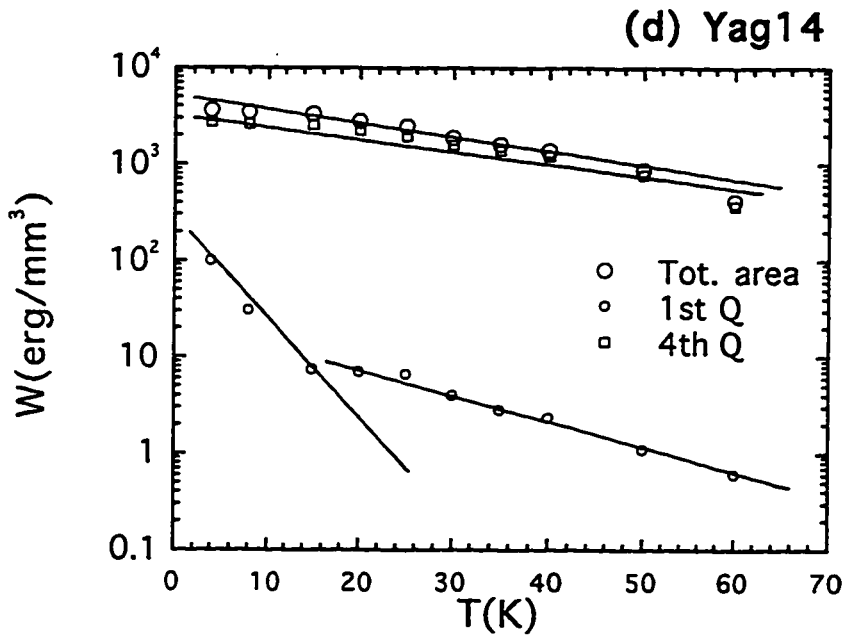
(d) Yag14
W(erg/mm^3)
10^4
10^3
10^2
10
1
0.1
0
10
20
30
40
50
60
70
T(K)
Tot. area
1st Q
4th Q

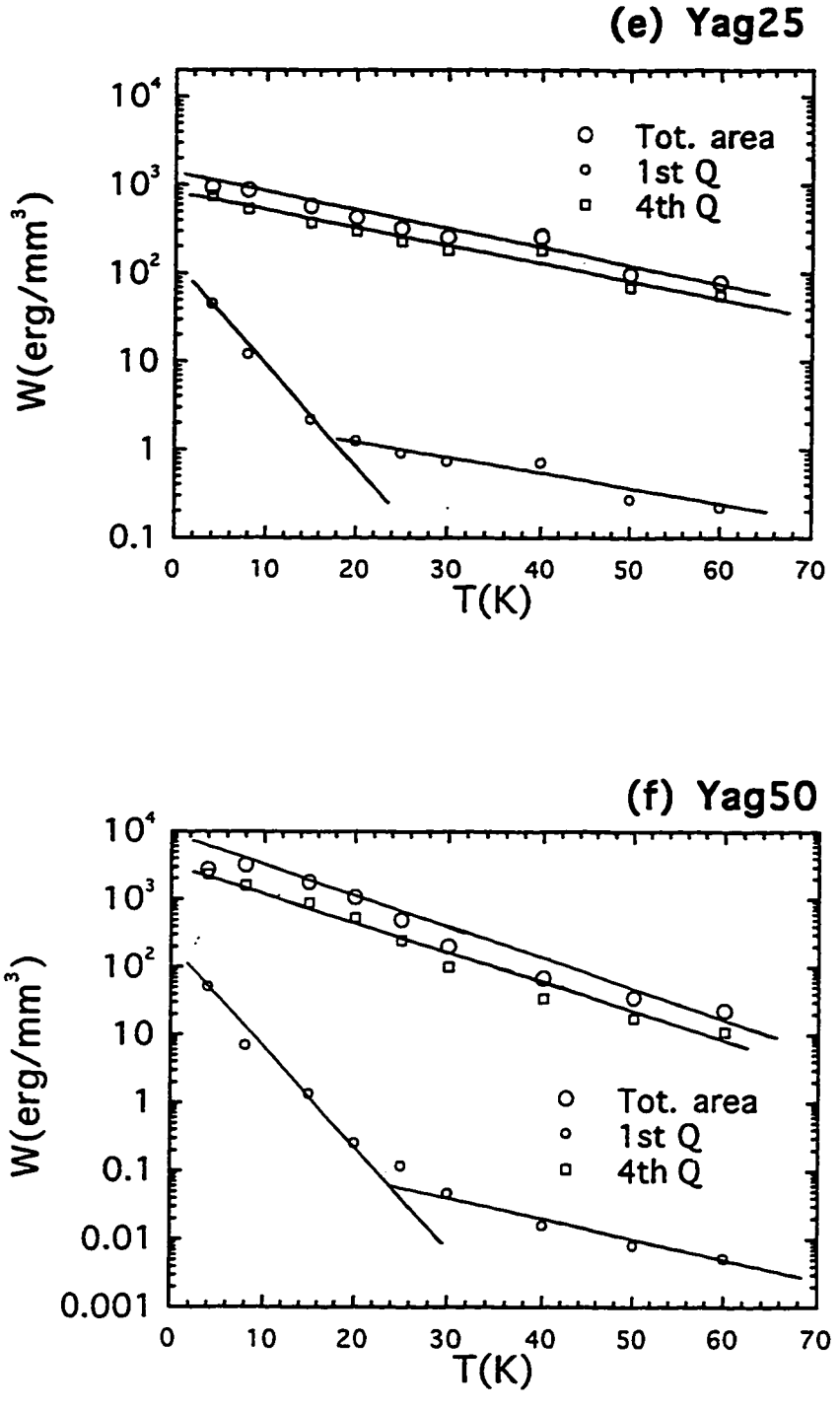

Figure 4.2: a,b,c,d,e,f : energy loss(trapped, diamagnetic, and total) for different temperatures.

Table 4.1: The variation of the exponent of the magnetic field where n1 and n2 represent the behaviour of the energy loss in the reigeons of law and high fields respectively

sample	n_1	n_2
Y123	1.39	1
YAg7	2.2	1
YAg10	2.41	1
YAg14	1.07	1
YAg25	1.083	1
YAg50	0.65	1

Table 4.2: The best linear fit in the energy vs temperature relation showing the trapped, diamagnetic contributions and the total energy for the different samples under the scope

sample	W_{trap}erg/cm^3	β_{trap}K^{-1}	W_{tot}erg/cm^3	β_{tot}K^{-1}	W_{dia}erg/cm^3	β_{dia}K^{-1}
Y123	7.27×10^5	0.188	8.24×10^6	0.038	5.32×10^6	0.036
YAg7	5.13×10^5	0.220	8.42×10^6	0.04	6.07×10^6	0.04
YAg10	9.17×10^5	0.241	10.54×10^6	0.03	9.00×10^6	0.03
YAg14	2.31×10^5	0.234	5.34×10^6	0.04	3.98×10^6	0.03
YAg25	0.89×10^5	0.226	1.117×10^6	0.05	7.82×10^6	0.05
YAg50	1.04×10^5	0.086	5.66×10^6	0.099	3.40×10^6	0.10

Chapter 5

Conclusion

The magnetic measurement were performed on high quality samples of polycrystalline $Y_1Ba_2Cu_3O_7/(Ag_2O)_x$ with x ranging between 0% and 50%. Hysteresis loops obtained at different fields ($0 \leq H \leq 9$ Tesla) and temperatures ($4.2 \leq T \leq 60K$) have been used to obtain the critical current density, pinning forces and the energy losses in accordance of the assumptions of Bean's Model. Generally, the critical current for all samples decrease with increasing magnetic field or temperature. However, the critical current is highest when silver oxide is added to Y123 with a concentration of 10%. It is higher than that of pure Y123 at H=0 and T=4.2K by about three times. The critical current initially decrease rapidly with increasing field reaching half of its initial value at H=2 Tesla, then exhibit a gradual decrease up to the maximum

applied field (9 Tesla). The effect of silver reveals a complete picture when x exceeds 10% to the maximum amount of 50% in our project. Degradation of the superconducting properties has been observed with samples that has $x \geq 10\%$ weight ratio of Ag_2O. The deterioration of the sample appear in the sample with x=25% and more clearly when x=50% where low values of the critical current and pinning forces have been observed..

The pinning forces mechanism is the cause behind the critical current. As the density of the pinning centers increase, more critical current can be carried by the sample. The critical current of Y_{Ag10} is maximum, because the pinning force in this sample is maximum. At T=30K, the pinning force of Y_{Ag10} is three times higher than that of the pure sample.

In addition, the pinning force is higher at low temperatures since the thermal energy available at higher temperature increase the possibility of the vortices to jump the pinning potential barrier.

Magnetic energy loss has been also investigated in the presence of DC-magnetic field unlike what is commonly done.

The energy loss is calculated through the area of the hysteresis loops. At T=4.2K, the energy loss is strongly field dependent for low fields and exhibiting a power low dependence $W \propto H^n$ in this region.. The value of n is found to have a maximum value of 2.2 for YAg10. However, at high fields, W saturates and

is nearly increasing linearly in that region.. So, in clear disagreement with Bean's model at low fields and in good agreement at high fields.

In addition, at low temperatures, the energy due to the trapped field in the sample is considerably large. As the temperature increase, the trapped flux lines leave the sample and the energy is mostly due to diamagnetism. The loss is highest for Y_{Ag10} as it is clear from Fig 4.2.

To conclude, the addition of silver oxide enhances the pinning mechanism and as a result the critical current as far as the concentration of the silver oxide is below 10%.

Bibliography

[1] A.C.Rose-Inns "Introduction to Superconductivity" (Pergamon, city, 1978).

[2] Kresin, V. Wolf, S.A "Fundamentals of Superconductivity" (Plenum, NY, 1990).

[3] M.K. Wu, J. R. Ashburn, C.J. Torng, P.H. Hor, R.L. Meng, L.Gao, Z.J. Huang, Y.Q. Wang and G.W. Chu, Phys. Rev. Lett. 58, 908 (1987).

[4] Ginsberg, D.M. "Physical Properties of High Temperature Superconductors" (World Scientific Pub.Co., 1989).

[5] Nasser M. Hamdan, A General Review on Superconductivity, METU (1988).

[6] J.B.Boyce, F. Bridges, T. Claeson, R.S. Howland and T.H. Geballe, Phys. Rev. B 36, 5251 (1987).

[7] R.M. Hazan, L.W. Finger, R.J. Angel, C.T. Prewitt, N.L. Ross, H.K. Mao and C.G. Hadidiacos P.H. Hor, R.L. Meng and C.W. Chu, Phys Rev. B 35, 7238 (1987).

[8] C Rossel and ϕFisher, Met. Phys. 14, 455(1984).

[9] Y.Yeshurun, I. Felner and H. Sompolinsky, Phys. Rev. B 36, 840 (1987).

[10] H.Ullmaier "Irreversible Properties of Type II Superconductors" (Springer-Verlag, Berlin, 1975).

[11] Abdelhadi, MM and Ziq Kh. A, Supercond. Sci. Technol. 7, 99 (1994).

[12] L.Martini, A. Ganadini, L. Rossi, V. ottoboni, S. Zannella, Physica C 235, 3033 (1994).

[13] M. Ciszek, J. Olegniczak, E. Trojnar, A.J. Zaleski, J. Klamut, A.J. M. Roovers and L.J. M. VAn De Klundert, Physica C 152, 247 (1988).

[14] K.H. Muller, C. Andrikidis. H.K. Liu and S.X. Dou, Physica C 247, 74 (1995).

[15] S. Zanella, L. Jansak, M. Majors, V.Selvamanickam and Salama, Physica C 205, 14 (1993).

[16] S. Zanella, J. Tenbrink, K.Heine, A. Ricca and G.Ripamonti, Appl. Phys. Lett 57, 192 (1990).

[17] L. Ganapathi, Ashok Kumar and J. Narayan, Mat. Res. Soc. (MRS), Symp. Proc. 169, 1267 (1990).

[18] L. Ryelandt ,M. Cassart, F. Delanny et al, Mat. Res. Soc. (MRS), Symp. Proc. 169, 1243 (1990).

[19] B. Dwir, M Affronte, and D. Pavuna, Appl. Phys. Lett. 55 (4), (1989).

[20] L. Civale, M.W. McELfresh, A.D. Marwich, F. Holtzberg, C. Field, J.R. Thompson and D.K. Christen, Phys. Rev. B 43, 13732, (1991).

[21] A. Fert, J.P. Redoules, Ph. Odier and N. Pellin, Physica C 235-240, 2908 (1994).

[22] M. Oussena, P. A. J. de Groot, A. Marshal and J.S. Abell, Phys. Rev. B 49, 1484 1994).

[23] L. Krusin-Elbaum, L. civale, V.M. Vinokur and F. Holtzberg, Phys. Rev . Lett 69, 2280 (1992).

[24] David R. Nelson, Phys. Rev. Lett 60, 1973 (1988).

[25] A. Houghton, R.A. Pelcovits and A. Sudbϕ, Phys. Rev. B 40, 6763 (1989).

[26] E. Rodriguez, C. Duran, J. Luzuriaga, F. de la Cruz and C. Fainstein, Physica C 165, 315 (1990).

[27] W. Jiang, N.C. Yeh, D.S. Reed, U. Kriplani, T.A. Tombrello, A.P. Rice and F. Holtzberg, Phys. Rev. B 47, 8308 (1993).

[28] R. Job and M. Rosenberg, Supercond. Sci. Technol. 5, 7 (1992).

[29] Matthew P.A. Fisher, Phys. Rev. Lett 62, 1415 (1989).

[30] Daniel S. Fisher, Matthew P.A. Fisher and David A. Huse, Phys. Rev. B 43, 130 (1991).

[31] S.Reich and D.Varetnik & I.Felner and U.Yaron, J. Appl. Phys. 72, 4805 (1992).

[32] M. Oussena, P. A. J. de Groot, R. Gagnon and L. Taillefer, Phys. Rev. B 49, 9222 (1994).

[33] M. Oussena, S. Porter, P. A. J. de Groot, R. Gagnon and L. Taillefer, Physica C 235-240, 2821 (1994).

[34] L. Ji, R. H. Sohn, G. C. Spalding, C. J. Lobb and M. Tinkham, Phys. Rev. B 40, 10936 (1989).

[35] C. P. Bean, Phys. Rev. Lett 8, 250 (1962).

[36] J. E. Evetts and P. H. Kes, Phys. Rev. Lett. 66, 1777.

[37] Charles P. Bean, Rev. Mod. Phys. 36, 31 (1964).

[38] K. A. Delin, T.P. Orlando, E.J. McNiff, Jr., S. Foner, R.B. van Dover, L.F. Schneemeyer and J.V. Waszczak, Phys. Rev. B 46, 11092 (1992).

[39] S.F.Kim, Z.Z. Li, H. Raffy, Physica C 244, 78.

[40] R.M. Schalk, G. Samadi Hosseinali, H.W. Weber, S. Proyer, P. Schwab, D. Bauerle, S. Grundorfer, Phys. Rev. B 49, 3511 (1994).

[41] L.W. Song, M. Yang, E. Chen and Y.H. Kao. Phys. Rev. B 45, 3083 (1992).

[42] K.H. Muller and A.J. Pauza, Physica C 161, 319 (1989).

[43] Yunhui, Weiyan Guan and K. Zeibig, Appl. Phys. Lett. 54, 1699 (1989).

[44] K.H. Muller, IEEE Transactions on Magnetics 27, 2174 (1991).

[45] S. Zannella, L. Jansak, M. Majoros, V. Selvamanickam and Salama, Physica C 205, 14 (1993).

[46] T. Fukunaga, S. Maruyama, T. Abe and A. Oota, Physica C 235, 3231 (1994).

[47] J. Orehotsky, Youwen Xu, Y.L. Wang, M. Garber and M. Suenaga, J. Appl. Phys. 67, 5461 (1990).

[48] Kazuo Kadowaki, S.L. Yuan, K. Kishio, T. Kitazawa, Phys. Rev. B 50, 7230 (1994).

[49] K. Kwasnitza, V. Plotzner, M. Waldmann and E. Widmer, Physica C 153, 1565 (1988).

[50] Kh. A. Zig, N. M. Hamdan and A.S. al Harthi, Physica C

[51] Kh. A. Zig, A. A. Pramana DN and M. Faiz, to be published.

[52] Astra A. P., MS Thesis, KFUPM, Phys. Dept. 1995.

[53] C. D. Wei, Z. X. Liu, Z. Z. Gan, Physica C 195, 286 (1992).